Heterogeneous & Homogeneous & Bio- & Nano-
CHEMCATCHEM
CATALYSIS

# Accepted Article

**Title:** The surface state and the catalytic performance of Co/CeO2 catalysts in the steam reforming of ethanol

**Authors:** Sylwia Turczyniak, Magdalena Greluk, Grzegorz Słowik, Wojciech Gac, Andrzej Machocki, and Spyridon Zafeiratos



**To be cited as:** *ChemCatChem* 10.1002/cctc.201601343

**Link to VoR:** http://dx.doi.org/10.1002/cctc.201601343

A Journal of
ChemPubSoc Europe

WILEY-VCH

www.chemcatchem.org

# The surface state and the catalytic performance of $Co/CeO_2$ catalysts in the steam reforming of ethanol

Sylwia Turczyniak,*[a,b] Magdalena Greluk,[a] Grzegorz Słowik,[a] Wojciech Gac,[a] Spyridon Zafeiratos,[b] and Andrzej Machocki[a]

**Abstract:** The effect of particles size, and addition of K promoter on the oxidation state of $Co/CeO_2$ was investigated and correlated with selectivity for the ethanol steam reforming (ESR) carried out with various $H_2O$/EtOH molar ratios. Spectroscopic studies showed that the oxidation state of catalysts components depends on the $H_2O$/EtOH molar ratio, and it changes with increasing water extent. It was found that surface oxygen-containing species (OH and $K^{\delta+}$–$O^{\delta-}$) are very important factors to achieve a good catalyst's selectivity, for lowering the amount of coke deposited and changing its nature from fully dehydrogenated C=C to $CH_x$. Beside surface concentration of oxygen-containing species, the catalyst's morphology and location where oxygen-containing species are chemisorbed may be equally important to their abundance – the selective ceria-supported cobalt catalyst should have well dispersed cobalt particles deposited on the well dispersed support.

## Introduction

In recent years cobalt-based catalysts for ethanol steam reforming (ESR) reaction have been in the focus of numerous studies seeking understanding the catalysts' function under working conditions. The aim is to provide rational improvement strategies so as to develop a low-cost, active and sustainable ESR catalyst [1]. Among the critical issues previously reported are *(i)* the effect of the initial state [2-5], *(iii)* the $H_2O$/EtOH molar ratio [6], *(iv)* reaction temperature [2, 5, 7, 8], *(v)* the influence of a support (i.e., surface acidity, morphology, particle size, oxygen-storing and releasing capacity and oxygen mobility) [3, 8-16], *(vi)* the nature of cobalt active sites [2, 4, 5, 7], *(vii)* the capability of cobalt [17-19], support [20, 21], and their interface to convert ethanol and water, and finally *(viii)* the role of alkali metal promotion [22-24].

The oxidation state of cobalt under the ESR reaction has been a subject of many studies [2, 3, 5, 7, 8, 10, 25-27]. The evidence for co-existence of both forms of cobalt (metallic and cobalt(II) oxide) under the reaction conditions has been provided by various techniques [2-5, 7, 8, 17, 19, 21, 26-31]. Recent density functional theory calculations on ethanol transformations on the surface of cobalt catalysts suggest, that while carbon monoxide and hydrogen are products more favourable on metallic cobalt species, acetaldehyde is the main final product on Co(II) sites [32]. The similar conclusion has been drawn from experiments in which a cobalt foil and cobalt oxide thin films were exposed to ethanol vapours [19]. Using model Co/ZnO catalysts, E. Martono et al. [33] and Y.T. Law et al. [34] also showed that metallic cobalt is active for ethoxide decarbonylation into carbon monoxide and hydrogen, while CoO provides the active sites for ethanol dehydrogenation. *In-situ* XPS studies of $Co/CeO_2$ [29] combined with *on-line* products analysis confirmed that also over real catalytic systems, in the presence of metallic form of cobalt only, carbon monoxide is the most favourable product. Even though the effect of cobalt oxidation state on catalytic performance has been widely investigated over unsupported [17, 18] and supported systems [28], as yet there is no consistency in what is the most active and selective form of cobalt under the ESR [35] and all combinations *(i)* a mixture of Co(0) and Co(II) [2, 4, 5, 33, 36, 37], *(ii)* metallic cobalt [4, 18, 26, 31, 28] or *(iii)* Co(II) [7, 23, 38, 39] have been proposed in the so far published results.

The role of a support is also of major importance and to date ceria-supported catalysts are considered to be one of the most promising systems [40]. This is assigned mainly to the facility of ceria to reversible change of its oxidation state between Ce(IV) and Ce(III) [41-42], and its remarkable oxygen storage capacity [15, 43-46]. Superior properties of ceria are believed to preserve the catalyst surface area (due to physical stabilisation of cobalt crystallites preventing them from sintering [15]) and the catalytic activity [15, 47]. It was shown that ceria may play an important role in modifying the formation of active cobalt species (for

[a] Dr. S. Turczyniak, Dr. M. Greluk, M.Sc. G. Słowik, D. Sc., Assoc. Prof. W. Gac, D.Sc., Assoc. Prof. A. Machocki
Faculty of Chemistry
Maria Curie-Sklodowska University in Lublin
3 Maria Curie-Skłodowska Square, 20-031 Lublin, Poland
E-mail: sylwia.turczyniak@poczta.umcs.lublin.pl
[b] Dr. S. Zafeiratos
Institut de Chimie et Procédés pour l'Energie, l'Environnement et la Santé (ICPEES), ECPM, UMR 7515 CNRS-Université de Strasbourg
25, rue Becquerel, 67087 Strasbourg Cedex 02, France

Supporting information for this article is given via a link at the end of the document.

example via release of lattice oxygen) [34, 48], dissociation of water [49, 50], transformation of ethanol [49, 51], and in altering the reaction pathways [13, 52, 53]). Not only the support nature is substantial in the overall ESR process. Another important factors influencing a catalyst's activity and selectivity are morphology and textural properties of the support [3, 13, 20].

I.I. Soykal and co-workers investigated the influence of particles size (3.5 nm and 120 nm) [3, 21], and morphology [11] on reducibility of ceria and its catalytic performance under the ESR. They found that whether ceria was pre-reduced or not, it converge to the same oxidation state (mixture of Ce(IV) and Ce(III)) at given temperature, and exhibited a similar ESR performance; however, a highly dispersed ceria produced much more ethylene than its low-dispersed counterpart [3, 21]. In contrast to the studies presented in ref. [3, 21], the results of A. M. da Silva et al. [54], and N. Laosiripojana and S. Assabumrungrat [20] showed that the low surface area ceria exhibited high selectivity to ethylene, whereas its high surface area counterpart was selective towards acetaldehyde [54]. However, the authors agreed [21, 54] that the nano-sized ceria ensures higher ethanol conversion and hydrogen yield. Therefore, discrepancy between the results of different teams [3, 8, 13, 21], while concerning the ESR carried out over $Co/CeO_2$, catalysts, may arise from differences in morphology and catalytic properties of used ceria support.

A great number of publication is focused on the role of cobalt and ceria oxidation state in the ESR [2, 3, 7, 8, 10, 11, 21, 29], whereas only in a few the attempt was made to explain the role of surface adsorbed hydroxyl species, or generally speaking surface adsorbed oxygen-containing species [44, 55-57]. The group of A.M. da Silva et al. [43] suggested that hydroxyls adsorbed on the ceria's surface assist in coke removal from cobalt, whereas another paper [1] higlight that a high concentration of surface adsorbed oxygen-containing species may also induce oxidation of metal surface. In the second case it is obvious that adsorbed species would influence a catalyst's selectivity [48], therefore, playing an important role in the ESR. S.M de Lima et al. [55] presented a scheme of ethoxy species transformation in which dehydrogenated species (acetyl species) undergo support-induced oxidation by oxygen-containing species (OH or surface oxygen adatoms) forming acetates. Acetate species can be further oxidized by surface adsorbed oxygen-containing species to carbonates followed by decomposition to carbon dioxide.

It is generally accepted that promoters improve the stability of catalysts. Promoters (e.g., alkali metals, such as sodium [58, 59], potassium [22-24, 31, 60-62] or noble metals, like rhodium [7, 10, 40, 63], platinum [62, 64]) are widely used to improve catalysts' activity [24, 59] and extent catalysts' lifetime by making sintering [47] and carbon formation [23, 24, 31, 59, 60] more difficult. The group of J.-W. Snoeck [65] examined the effect of potassium loading on nickel-catalysts on the rate of carbon gasification. Their findings showed that the most satisfying results were obtained with 1.6–2 wt.% of $K_2O$ content. Besides, S. Ogo et al. [23] showed that 1–2 wt.% potassium addition improved both the activity and selectivity of the $Co/Al_2O_3$ catalyst, which stays in line with results of other researchers [22, 24, 60]. The authors [23] deduced that beneficial properties of potassium addition are related to the reduction of Co(II) into Co(0), stabilization of acetate species, and suppression of methane formation. In some studies potassium was also found to prevent ethylene formation [31], which is well-known coke precursor [9, 66], consequently hindering coke formation.

The catalyst's stability is in the core of the effort to develop new, advanced catalysts for the ESR. Although $Co/CeO_2$ catalysts are very promising candidates for the ESR they exhibit loss of the activity and selectivity in long-testing experiments, even after alkali metal promotion, which is commonly attributed to coke deposition. Apart from the use of alkali promoters, the increase of the water to ethanol molar ratio in the feed can be also used to moderate carbon accumulation with time-on-stream [6]. K. Vasudeva et al. [67] suggested that carbon formation on catalysts' surface occurs only at low $H_2O$/EtOH molar ratios (<2/1), whereas the group of V. Mas [68], that the $H_2O$/EtOH = 3/1 mol/mol and T>230°C are required to avoid coke formation. Other group of researchers [69] implied that the steam to carbon molar ratio up to 10/1 is needed to obtain the best production of hydrogen, minimize the formation of carbon monoxide and methane, and to avoid carbon deposition.

Although cobalt-based catalysts have been in the focus of many research groups, there are no works dealing with more than one or two variable factors at a time. Moreover, there were no attempts to use surface sensitive methods to characterize potassium-promoted $Co/CeO_2$ systems under the different $H_2O$/EtOH molar ratios. In this study catalysts of similar chemical composition, but completely different properties were used deliberately, as in ref. [3, 8, 13, 21]. The present work aims to

show the influence of the above factors in a holistic approach focusing mainly on the surface state. The main objectives of this study was to find *(i)* cobalt and ceria oxidation state after activation in hydrogen and after the ESR, *(ii)* the effect of the ceria support and cobalt active phase particles size on catalyst's reducibility and its behaviour in the ESR, *(iii)* the effect of potassium promotion on the catalyst's surface state after reduction and the ESR, *(iv)* the influence of the $H_2O$/EtOH molar ratio on the surface state of the quenched $Co/CeO_2$ catalysts, and *(iv)* the impact of the $Co/CeO_2$ catalysts' surface state on their catalytic performance in the ESR.

## Results

### *1.1. Reduction of the catalysts in hydrogen*

As shown in Table 1 the BET surface area of HS- and LS-catalysts differs by about one order of magnitude, but after addition of potassium the surface area of the HS-catalyst decreases considerably. In addition, although cobalt wt.% content is comparable in all catalysts (8–9 wt.%),the cobalt surface area is significantly higher for the HS-catalyst (47.2 $m^2$/g) as a result of much lower cobalt particle size (3.8 nm). The potassium promotion increases average cobalt particle size (13.9 nm) and lowers cobalt surface area (4.1 $m^2$/g) as compared to the unpromoted HS-catalyst, making it comparable to ones obtained for the LS-catalyst (1.5 $m^2$/g). However, one should note that cobalt crystallites in the LS-catalyst were much bigger (39.3 nm) as compared to the other catalysts.

The reducibility of cobalt oxides is strongly related to the cobalt crystallite size [3, 8, 21], as well as to the presence of additives [7, 22, 40, 61-63]. Large cobalt oxide particles were expected to reduce more easly than the smaller ones [13, 70]. Therefore, on the basis of cobalt oxide crystallite size (Table 1) the reduction of the HS-catalyst at higher temperature can be rationalized. In the presence of potassium, additional effects might influence the reducibility of the catalyst apart from the cobalt crystallites size.

Fig. 1 shows the XPS core level spectra of the elements found over the catalyst's surface after reduction at 420°C in hydrogen (detailed characterization of the pristine samples can be found in the Supplementary Information, Fig. S1). For quantification of the data, the collected Ce 3d high resolution spectra (Fig. 1a) were curve fitted [29, 71] with combination of two reference spectra of Ce(IV) (****) and Ce(III) (***III***) recorded over cerium(IV) oxide and hexahydrate cerium(III) nitrate, as suggested in ref. [8]. The peak fitting procedure of references is presented in Supplementary Information, Fig. S2. The peaks position, full width at half maximum were constrained as proposed in ref. [8]. Similarly, two components recorded on reference samples were also used for Co $2p_{3/2}$ (Fig. 1b) fitting: one for metallic cobalt (***III***), located at 778.6 eV, and a second around 781.4 eV – formally ascribed to oxide-like component (CoO and/or Co–OH) (****). As similar to ceria references, the fitting procedure of cobalt references (based on ref. [72]) has been presented in Supplementary Information, Fig. S3. In literature [72] metallic cobalt is fitted with a characteristic asymmetric main peak and two plasmon loss peaks (located at 3.0 and 5.0 eV higher binding energy than the main component), origination of which was explained elsewhere [72]. From Fig. 1(a-b) it is evident, that after hydrogen treatment the surface of all catalysts was reduced, however, to a different extent. It should be pointed out that in Fig. 1b the intensity of the fitted Co(II) component is comparable to the noise level of the spectra, therefore the error bars in determined Co(II) percentage contribution might be encumbered with a meaningful error. The obtained spectra proved that similarly to *in-situ* XPS studies [2, 3,

**Table 1.** Results of the $Co/CeO_2$ catalysts characterization

| Catalyst | BET surface area, $m^2/g$[a] | Volumes of pores, $cm^2/g$[a] | Pore diameter, nm[a] | Cobalt content, wt.%[b] | Average crystallite size, nm[c] | | Average cobalt crystallite size, nm[d] | Cobalt dispersion, %[d] | Cobalt surface area, $m^2/g_{cat.}$[d] |
|---|---|---|---|---|---|---|---|---|---|
| | | | | | $Co_3O_4$ | $CeO_2$ | | | |
| LS-$Co/CeO_2$ | 5.3 | 0.03 | 28.2 | 9.00±0.27 | 23.3 | 87.1 | 39.3 | 2.5 | 1.5 |
| HS-$Co/CeO_2$ | 47.2 | 0.15 | 11.0 | 9.55±0.38 | 8.4 | 25.6 | 3.8 | 26.6 | 17.1 |
| HS-K$Co/CeO_2$ | 29.6 | 0.12 | 12.4 | 8.44±0.34 | 9.3 | 26.5 | 13.9 | 7.2 | 4.1 |

[a] Determined by the low-temperature $N_2$ adsorption. [b] Determined by XRF. [c] Determined by XRD. [d] Determined by the hydrogen chemisorption measurements.

8, 25, 29], and in contrast to so far published *ex-situ* XPS studies [7, 10, 40] it is possible to efficiently maintain cobalt mainly in a metallic form, if it predominates.

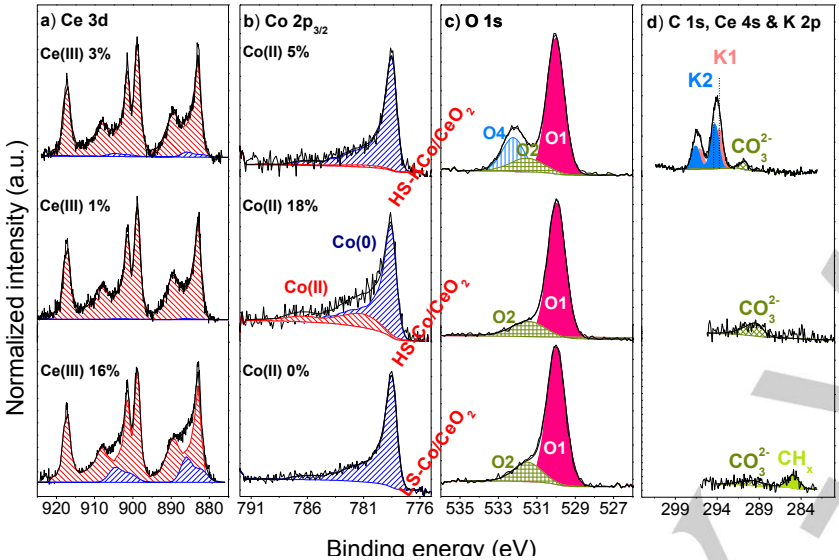


**Figure 1.** The high resolution XPS spectra of Ce 3d (a), Co $2p_{3/2}$ (b), O 1s (c) and C 1s, Ce 4s & K 2p (d) collected after the reduction ($H_2$/Ar= 50/50 $cm^3$, T = 420°C, $p_{total}$ = 1 atm, 1 h) of the LS-Co/$CeO_2$, HS-Co/$CeO_2$ and HS-KCo/$CeO_2$ catalysts; a) Ce(IV) (\\\), Ce(III) (*///*), b) Co(II) (\\\), Co(0) (*///*), c) O1 – lattice oxygen, O2 – hydroxyl and carbonate species, O4 – carbonate species bounded to potassium, d) probable assignments of K1 and K2 species can be found in the text.

Results show complete reduction of cobalt oxides on the surface of the LS-catalyst (within experimental error, therefore it cannot be excluded that traces of the $CoO_x$ phase do not exist), while on the HS and HS-K traces of $CoO_x$ remain after the hydrogen treatment. The presented XPS results are in a good agreement with the TPR profiles shown in the Supplementary Information Fig. S4. The reduction behaviour of nano- and micro-Co/$CeO_2$ was also examined by I.I. Soykal et al. [3], whose *in-situ* X-ray absorption fine structure spectroscopy studies demonstrated that the extent of cobalt oxides reduction was higher with the nano-Co/$CeO_2$ catalyst. The result was attributed, by the authors, to the small particles size and high dispersion of the sample. This is somewhat counterintuitive, since is admitted that smaller cobalt oxide particles are more difficult to reduce than larger one [13, 70, 73]. Some authors postulate that persistent Co(II) species can be a result of a strong metal-support interaction [13, 73], slight encapsulation [10], and/or penetration $Co^{2+}$ ions into the support lattice [40, 74].

It is well known that pure ceria is difficult to reduce in hydrogen at relatively low temperatures [40, 75, 76], however, in the presence of cobalt (or other metal) it can be partially reduced due to hydrogen *spill-over* effect [13, 44, 75, 77-79]. Recently it has been shown that the reduction degree of ceria (average size of ceria crystallites was 4 nm) in the Co/$CeO_2$ might be lower than that of a bare ceria support [8], and this effect is dictated by the temperature.

The new features appearing on the Ce 3d spectra, shown in Fig. 1a, indicate that the ceria support of the LS-catalyst was partially reduced Ce(III) = 16%, while the supports of promoted and unpromoted HS-catalysts remained almost fully oxidized. The evolution of Ce 3d spectra, in reducing conditions has been widely studied by many authors [21, 41, 79-85]. Higher diffusion ability of oxygen atoms for the HS-ceria support due to the higher defects' concentration leads to the different reduction level between the HS-ceria and LS-ceria [41].

The O 1s spectra (Fig. 1c) of the unpromoted catalysts are very similar. The detailed information of each component contribution in the overall spectra can be found in Supplementary Information – Table S1. The main peak (530 eV) can be safely assigned mainly to the ceria lattice oxygen (O1) [86-89] (however, in literature at this binding energy the lattice oxygen in $CoO_x$ was also recorded [19]), while the assignment of the high binding energy component at 531.5 eV (O2) is controversial. Some authors assign it directly to the presence of –OH groups [90-93], others rather generally identify them as adsorbed oxygen ions ($O^-$ species) on surface oxygen vacancies [87, 94, 95]. Quite recently Z. Liu et al. [86] came up with the proposal that in ceria-supported systems the peak located at 1.4 eV higher binding energy than the main oxygen component is probably related to the ceria hydroxide layer $Ce^{3+}(OH)_x$. On the spectra of the potassium-promoted catalyst, an additional peak at 532.2 eV (O4) was found. In literature this peak is regarded as the fingerprint of the presence of amorphous layer of potassium oxides [96], potassium hydroxide [97], or potassium carbonate [98, 99].

The presence of amorphous potassium oxides on the surface of the ESR catalysts was recently confirmed by S. Ogo et al. [23]. The nature of potassium oxides is still under discussion. B. Lamontagne et al. [110] have studied the alkali

metal promotion on silicon oxidation and their measurements revealed the existence of four potassium oxides formed during increasing oxygen exposure. They assigned the peak at 531.0 eV to $K_2O_2$, 532.0 eV to $K_2O_3$ and 534.2 eV to $KO_2$. Contrary, G. Pirug et al. [101] have assigned the component at 531.7 eV to $K_2O_2$ surface species. Z. Hou et al. [97] have suggested KOH as a form of potassium on the surface. According to M. Carlsson [102] potassium forms hydroxide species resulting in the increase of the surface basicity. In further part of this paper we will try to shed a light on the nature of K1 and O4 components.

Before reduction, carbonaceous deposit was detected on the surface of all catalysts (Supplementary Information, Fig. S.1). The reduction procedure allowed for the removal of adsorbed carbon impurities and purification of the surface (Fig. 1d). For the K-promoted catalyst the peaks at 294.3 and 297.0 eV are definitely related to presence of $K^+$ ions (K 2p core level). The intensity of these peaks increased after hydrogen pre-treatment (Fig. 1d), as compared to the calcined sample (Supplementary Information, Fig. S1d). The calculated percentage contribution of potassium on the surface of the fresh sample was 3.2 at.%, whereas after reduction – 17.8 at.% (Table 2), suggesting surface's enrichment in potassium (its re-dispersion) after reduction. Analysis of the K 2p region (Fig. 1d) allowed to observe a small asymmetry and the shift of the peak (the K $2p_{3/2}$ components located at 293.8±0.2 and 294.6 ± 0.2 eV respectively were denoted as K1 and K2) towards higher binding energies (BE), as compared to further results (Fig. 2d-4d).

Even though the chemical nature of potassium species is not clear yet, it is convincing that potassium state would depend on the local chemical environment of the surface [104], as well as that potassium species can be transformed one into another. In the view of the above discussion, in this work the shift of the K 2p (appearance of the component K2) towards slightly higher BE's is suggested to be ascribed to the change of electronic properties of potassium.

H.P. Bonzel et al. [103, 104] have presented the results of XPS studies of K-promoted surface of the Fe foil and suggested that the presence of K $2p_{3/2}$ component around 294 eV and oxygen at 532.2 eV is strongly supporting the hypothesis of KOH existence [103], however, only in the case of absence of the carbonate peak at ~290 eV [104]. In the presence of carbonates the oxygen peak at 532.3 eV can be assigned also to the existence of potassium carbonates [98]. It should be noted that BE's of the K $2p_{3/2}$ for as deposited $KNO_2$, $K_2CO_3$ and KOH films on the Fe foil were very close (293.7–293.8 eV) and the shift towards higher BE's (293.9–294.1 eV) were observed after samples' reduction [103, 104]. Accoring to the work of G. Maniak et al. [105] regardless of potassium compound used for cobalt oxide promotion, shifts on the BE scale are not observed. Basing on this observation, we assigned the K1 component to all potassium bonded to oxygen species.

**Table 2.** The percentage contribution (at.%) of elements on the surface of catalysts under the ESR (calculated on the basis of high resolution XPS spectra after taking into account the atomic sensitivity factor of each element)

| Catalyst | $H_2O$/EtOH (mol/mol) | Contribution of element (at. %)[a] | | | | |
|---|---|---|---|---|---|---|
| | | Co | Ce | O | C | K |
| LS-Co/$CeO_2$ | $H_2$[b] | 17.358 | 22.412 | 49.184 | 11.046 | - |
| HS-Co/$CeO_2$ | | 7.935 | 26.334 | 54.070 | 11.661 | - |
| HS-KCo/$CeO_2$ | | 4.388 | 17.825 | 54.171 | 5.775 | 17.842 |
| LS-Co/$CeO_2$ | 3/1 | 0.779 | 1.490 | 3.877 | 93.854 | - |
| HS-Co/$CeO_2$ | | 1.963 | 4.121 | 9.471 | 84.445 | - |
| HS-KCo/$CeO_2$ | | 1.680 | 13.443 | 47.475 | 22.154 | 15.248 |
| LS-Co/$CeO_2$ | 9/1 | 15.871 | 17.588 | 60.571 | 5.969 | - |
| HS-Co/$CeO_2$ | | 4.374 | 18.277 | 46.313 | 31.035 | - |
| HS-KCo/$CeO_2$ | | 1.322 | 9.227 | 50.441 | 13.657 | 25.353 |
| LS-Co/$CeO_2$ | 12/1 | 18.882 | 18.090 | 60.438 | 2.590 | - |
| HS-Co/$CeO_2$ | | 7.549 | 23.183 | 56.136 | 13.132 | - |
| HS-KCo/$CeO_2$ | | 0.818 | 4.384 | 48.687 | 13.255 | 32.856 |

[a] Calculated as: $n_i = n_i/\sum n_{i-j}\cdot 100\%$, where $n_i$ = {Co, Ce, O, C, K} and $n_{i-j}$ = Co+Ce+O+C+K. [b] Results obtained after the catalysts' pre-reduction ($H_2$/Ar) at 420°C for 1 h.

### *1.2. XPS characterization of catalysts after the ESR with a stoichiometric $H_2O$/EtOH molar ratio*

The XPS results recorded after the ESR reaction at a stoichiometric (3/1 mol/mol) $H_2O$/EtOH molar ratio (T = 420°C, $p_{total}$ = 1 atm, t = 1 h), show partially reduced ceria support and metallic cobalt with traces of $CoO_x$ (Fig. 2a and 2b). It is interesting to note that as compared to the state prior to the ESR (reduced samples, Fig. 1), the stoichiometric reaction mixture seems to be more efficient in ceria's reduction than hydrogen, which is in agreement with previous reports [25, 36]. On the other hand, it is different for cobalt, since its oxidation state remains almost the same as before the reaction (please compare Fig. 1b and 3b). Our previous *in-situ* XPS studies of the nano-Co/$CeO_2$ catalyst, carried out for the $H_2O$/EtOH molar ratio of 3/1 (420°C, $p_{total}$ = 0.2 mbar) [29] revealed that whereas

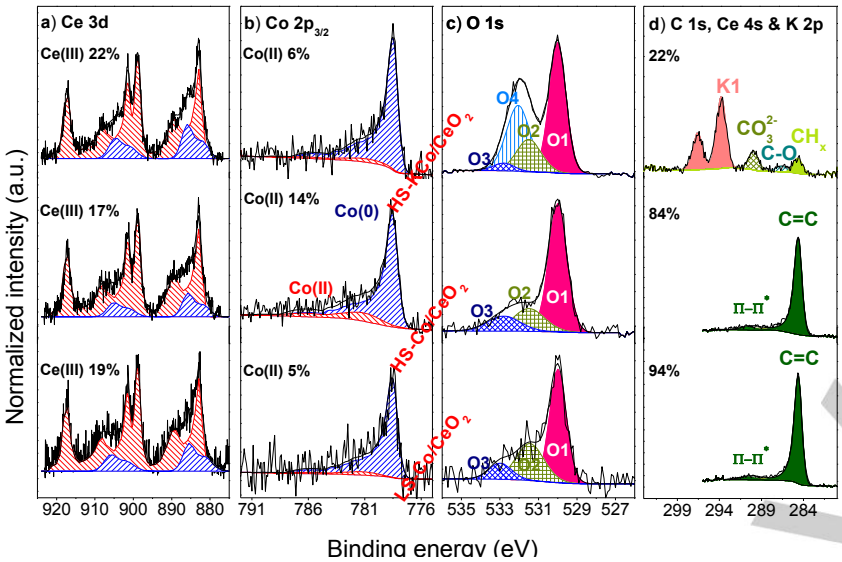


**Figure 2.** The high resolution XPS spectra of Ce 3d (a), Co $2p_{3/2}$ (b), O 1s (c) and C 1s, Ce 4s & K 2p (d) collected after the ESR ($H_2O$/EtOH = 3/1 mol/mol, T = 420°C) over the pre-reduced ($H_2$, T = 420°C) LS-Co/$CeO_2$, HS-Co/$CeO_2$ and HS-KCo/$CeO_2$ catalysts; a) Ce(IV) (\\\), Ce(III) (*///*), b) Co(II) (\\\), Co(0) (*///*), c) O1 – lattice oxygen, O2 – hydroxyl and carbonate species, O3 – water, O4 – carbonate species bounded to potassium, d) K1 – potassium carbonate. On the picture (d) also the percentage atomic contribution of carbon on the surface was given.

ceria's oxidation state was influenced by the conditions (hydrogen or ESR reaction mixture), cobalt oxidation state remained the same. It is also worth to mention about the results of *ex-situ* XPS studies carried out over the pre-reduced 10% Co/$CeO_2$-$ZrO_2$ catalyst, exposed to the slightly higher $H_2O$/EtOH molar ratio (4/1 mol/mol, 450°C) revealed re-oxidation of metallic cobalt to $CoO_x$ accompanied by ceria's reduction [36].

The higher reduction degree of ceria, as calculated based on Ce 3d spectra, was found for the HS-K catalyst (22% of Ce(III)). In addition, as compared to the unpromoted HS-catalyst, cobalt of HS-K catalyst is more reduced (Co(II) = 5%). Previous reports of L. del Río et al. [38, 106] demonstrated that in the ESR reaction ($H_2O$/EtOH ≈ 6/1 mol/mol) at low temperatures (300–350ºC) potassium loading prevents cobalt oxides reduction to the metallic phase, whereas our studies provided the evidence that in fact it facilitates catalyst's reduction in the ESR reaction at higher temperature (420ºC). However, based on available publications concerning potassium-promoted catalysts [23, 60], there are some presumptions that similarly to ZnO promoter [26, 107], depending on the type of the support, potassium may promote or hinder cobalt oxidation in the ESR.

Comparison of the O 1s spectra of the samples after hydrogen pre-treatment (Fig. 1c) and the ESR reaction (Fig. 2c) shows, that the relative intensity of the O2 component (531.5 eV) increases, and a new component located around 532.8 ±0.2 eV (denoted as O3), appears. According to its binding energy the O3 component can be assigned to surface adsorbed water species [87, 108, 109]. Moreover, the concentration of surface adsorbed hydroxyl species (O2) is clearly higher for the LS and HS-K catalysts.

The unpromoted catalysts after 1 h of the ESR were covered by carbon deposit, as seen in the C 1s region (Fig. 2d). The C 1s peak position at 284.6 eV, as well as its characteristic asymmetric shape, indicates for the presence of graphitic carbon species [110]. The higher binding energy component (289.4 eV) is characteristic for both Ce 4s region [84], carbonate-type species [86, 104] and even carboxylates [86]. Carbon dominates the surface with 94% and 84% atomic concentration for the LS- and HS-catalysts, respectively (Table 2). Potassium inhibits carbon deposition (formation of C=C and $CH_x$ species) down to <10%; however, a new peak at 290 eV indicates for the presence of $CO_3^{2-}$ species (total carbon-containing species coverage including carbonates was <22% as shown in Table 2). The K 2p spectrum of the HS-K catalyst shows a doublet at 293.8 and 296.6 eV which is very close to the BE of the K 2p doublet (293.9 and 296.6 eV), recorded by E. de Smit et al. [111]. In this case the peak was assigned to metastable basic potassium carbonate species.

Potassium containing species are rather difficult to characterize, especially when they are highly dispersed [112, 113], therefore, knowledge about them is limited [112]. Nevertheless, it is worth to made an attempt to shed a light on their nature. The noticeable intensity increase of the C 1s peak at 290 eV allows to suppose that the K1 component is at least partially related to the presence of potassium carbonates, e.g., $2K^+CO_3^{2-}$ or $K^+CO_2^-$. Simultaneously with the increase of the K 2p signal intensity, the O4 signal intensity was increasing (Fig. 2c and 2d). Further application of the same reasoning lead one to expect that the O4 component in the O 1s overall spectrum might be related to potassium bound to oxygen from carbonate species (further abbreviated $K^{\delta+}$–$O^{\delta-}$). In order to shed a light on the origination of both K1 and O4 components, the high-

resolution XPS spectra of $K_2CO_3$ (pure for analysis, ≥99.0%) reference sample were collected. The experimentally derived data were used as a reference in calculating K 2p/$CO_3^{2-}$/O 1s ratio related to potassium carbonate species. Since in cerium containing systems the Ce 4s region is overlapping with C 1s signal, the contribution of the percentage the surface adsorbed $CO_3^{2-}$ species on the surface of catalyst was performed after subtraction of the Ce 4s impact on this component. The experimentally derived data led to the conclusion that the K 2p and O4 components are related to potassium carbonates.

### *1.3. XPS characterization of catalysts after the ESR at high $H_2O$/EtOH molar ratios*

The catalysts' resistance to coke formation can be improved by increasing water to ethanol molar ratio in the reaction feed [68, 69, 114]. In Fig. 3 the XPS spectra of catalysts in the $H_2O$/EtOH = 9/1 mol/mol mixture are shown. The surface of the unpromoted catalysts is more oxidized as compared to the 3/1 molar ratio. After the ESR carried out for the $H_2O$/EtOH molar ratio of 9/1 the Ce(III) ions surface concentration for was 14% and 11% for the LS- and HS-catalyst respectively, while the concentration of Co(II) species increases considerably (16.4% and 30.3% of Co(II) for LS- and HS-catalyst). The *in-situ* XPS studies of H. Sohn et al. [8], devoted to the ESR reaction ($H_2O$/EtOH = 9/1 mol/mol, 450ºC) over the nano- and micro-$Co/CeO_2$ led to the similar conclusion, that higher amounts of $CoO_x$ phase were detected on the surface of micro-dispersed catalyst. From the other hand, in contrast to our work, in the cited publication [8] it was found that the surface of nano-ceria was more reduced than the surface of the sample with larger particles size. Higher concentration of Ce(III) on the surface of the nano-ceria was assigned to the higher lattice strain in smaller particles [115, 116]. At the HS-K catalyst the $H_2O$/EtOH molar ratio of 9/1 also induces more oxidized cobalt, but notably has the reverse effect on cerium, which is more reduced than in the molar ratio of 3/1. In addition, the atomic fraction of potassium (Table 2) increases considerably followed by simultaneous increase of the O 1s component at 532.2 eV (Fig. 3c). The excess of water had a beneficial effect on suppression of carbon formation. The carbon atomic fraction, which was 94 - 84% in the $H_2O$/EtOH = 3/1 molar ratio, drops down to 6 and 31% for the LS- and HS-catalysts, respectively. However, one should note that the given carbon percentage contribution is considered to the whole C 1s core level, meaning that C=C, $CH_x$, and chemisorbed C–O and $CO_3^{2-}$ species are included. Potassium addition decreases the carbon fraction at the HS-K catalyst from 22% (for HS) to 14%, while the sole C 1s component around 290 eV (Fig. 3d) is characteristic for carbonate and carboxylate species as discussed in the previous section.

Further increase of the $H_2O$/EtOH molar ratio to 12/1 (Fig. 4) induces cobalt oxidation (34% of Co(II)) similar for both LS- and HS-catalysts, thus it might be concluded that water content has a limited effect on cobalt re-oxidation process [29, 36]. In the case of the HS-K catalyst, the Co 2p peak has been in the signal noise level after 1 h of the ESR, indicating that cobalt particles were buried underneath a thick layer (around 3 to 4 nm) which attenuates Co 2p signal. The intense signal of the K1 (K 2p) and O4 (from the O 1s) components suggests that cobalt particles were most probably covered by potassium bonded to oxygen layer (K–O). The Ce 3d peak was also barely detectable,

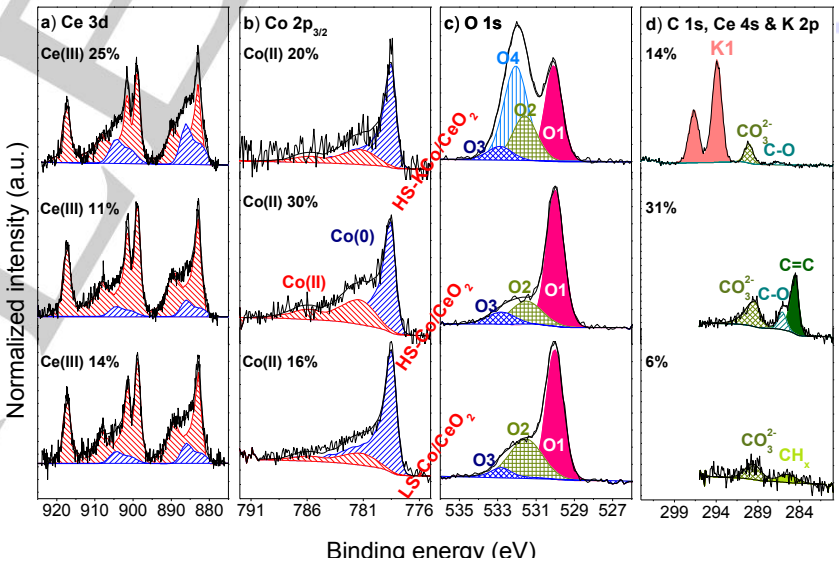


**Figure 3.** The high resolution XPS spectra of Ce 3d (a), Co $2p_{3/2}$ (b), O 1s (c) and C 1s, Ce 4s & K 2p (d) collected after the ESR ($H_2O$/EtOH = 9/1 mol/mol, T = 420°C) over the pre-reduced ($H_2$, T = 420°C) LS-$Co/CeO_2$, HS-$Co/CeO_2$ and HS-K$Co/CeO_2$ catalysts; a) Ce(IV) (\\\), Ce(III) (***///***), b) Co(II) (\\\), Co(0) (***///***), c) O1 – lattice oxygen, O2 – hydroxyl and carbonate species, O3 – water, O4 – carbonate species bounded to potassium, d) K1 – potassium carbonate. On the picture (d) also the percentage atomic contribution of carbon on the surface was given.

indicating that K–O is deposited without apparent distinction over cobalt and ceria support. In order to estimate the time-dependence of the K–O layer formation, the ESR at shorter reaction period (15 min) was carried out (inset of Fig. 4b). In this case the Co 2p signal directly suggests that K–O layer was thinner than after 1 h of the ESR, therefore its formation is time-depended.

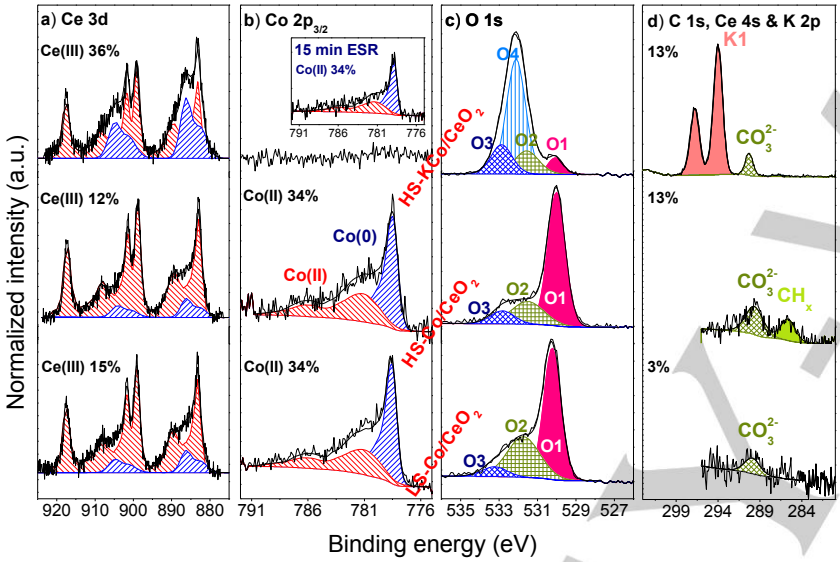


**Figure 4.** The high resolution XPS spectra of Ce 3d (a), Co $2p_{3/2}$ (b), O 1s (c) and C 1s, Ce 4s & K 2p (d) collected after the ESR ($H_2O$/EtOH = 12/1 mol/mol, T = 420°C) over the pre-reduced ($H_2$, T = 420°C) LS-Co/$CeO_2$, HS-Co/$CeO_2$ and HS-KCo/$CeO_2$ catalysts; a) Ce(IV) (\\\), Ce(III) (*///*), b) Co(II) (\\\), Co(0) (*///*), c) O1 – lattice oxygen, O2 – hydroxyl and carbonate species, O3 – water, O4 – carbonate species bounded to potassium, d) K1 – potassium carbonate. On the picture (d) also the percentage atomic contribution of carbon on the surface was given.

Our experiments show that for the HS-K catalyst more potassium species were observed in water rich reactants mixtures, suggesting segregation of potassium due to its stronger affinity to water. These experiments also allow us to conclude that the oxidation state of cobalt is the same like for the unpromoted catalysts (34% of Co(II)). Ceria valence state for the LS- and HS-catalysts were similar to this recorded for the 9/1 molar ratio, while deeper reduction of cerium oxide was found for the potassium-promoted catalyst (36% of Ce(III)).

The common feature for all catalysts was decreasing carbon deposition in water-rich reactants mixtures. It is worth to note that at the 12/1 $H_2O$/EtOH molar ratio, the promoted HS-K catalyst shows higher carbon atomic fraction (Table 2) as compared to the unpromoted catalysts. It can be explained by the lower surface potential barrier of potassium-covered surfaces [104] which increases the adsorption energy of carbon monoxide. Adsorbed species were converted on the surface into carbonate-type species.

The presented results show that regardless of the $H_2O$/EtOH ratio, a mixed metallic-ionic form of cobalt is always present on the surface during the ESR reaction. As expected, the concentration of Co(II) species was higher while the samples were exposed to the mixtures with higher than stoichiometric, reactants molar ratio. Oxidation of cobalt in the excess of water has been reported previously for Co/$Al_2O_3$ catalysts tested under $H_2O$/EtOH = 6/1 mol/mol [5], as well as for the Co/$CeO_2$-$ZrO_2$ with the $H_2O$/EtOH molar ratio of 4/1 [36]. The higher excess of water allows for higher concentration of surface adsorbed –OH groups (O2) (as compared to the results obtained in the stoichiometric ratio of reactants), facilitating carbon removal.

*1.4. The ESR catalytic performance of the catalysts*

Apart from the LS-catalyst at 3/1 molar ratio, the complete conversion of ethanol is achieved in all cases, after 1 h at 420ºC in a fixed-bed reactor. Water conversion at 3/1 molar ratio is between 37% and 54%, which is significantly lower than this expected from the ESR stoichiometry (100%). This indicates that non-selective ethanol transformations (without the participation of water molecules) occurred under the examined conditions. In the case of the ESR carried out in water excess (9/1 and 12/1 mol/mol), the water conversion over the LS- and HS-catalysts is close to the expected reaction stoichiometry (33% and 25%).

Table 3 shows the reactants conversions and the ESR reaction products selectivity obtained after 1 h at 420°C under all three $H_2O$/EtOH molar ratios. They are also close to those, measured in a high pressure flow reactor, used in the UHV system. Under all $H_2O$/EtOH molar ratios the ESR reaction products include $H_2$, $CO_2$, CO, $CH_4$ and some amounts of acetaldehyde observed only on the surface of LS-catalyst. Over all catalysts samples the selectivity to hydrogen was quite high and in general it increased with the increase of water excess,

varying between 82% (3.16 $mol_{H_2}/mol_{EtOH}$) and 98% (5.56 $mol_{H_2}/mol_{EtOH}$).

**Table 3** The selectivity of the ESR towards gaseous products, and yield of hydrogen and carbon dioxide after 1 h under the ESR at 420°C

| Catalyst | $H_2O$/EtOH (mol/mol) | Selectivity (%) | | | | | $H_2$/EtOH (mol/mol) | $CO_2$/EtOH (mol/mol) |
|---|---|---|---|---|---|---|---|---|
| | | $H_2$ | $CO_2$ | CO | $CH_4$ | MeCHO | | |
| LS-Co/$CeO_2$ | | 82.5 | 52.6 | 19.7 | 15 | 6.3 | 3.16 | 1.05 |
| HS-Co/$CeO_2$ | 3/1 | 84.6 | 67.2 | 10.6 | 22.2 | 0 | 4.03 | 1.34 |
| HS-KCo/$CeO_2$ | | 98.5 | 91.7 | 5.5 | 2.7 | 0 | 5.55 | 1.85 |
| LS-Co/$CeO_2$ | | 94.1 | 80.4 | 10 | 9.6 | 0 | 4.83 | 1.61 |
| HS-Co/$CeO_2$ | 9/1 | 95.1 | 86.5 | 5.7 | 7.8 | 0 | 5.19 | 1.73 |
| HS-KCo/$CeO_2$ | | 98.4 | 90.7 | 6.6 | 2.7 | 0 | 5.55 | 1.85 |
| LS-Co/$CeO_2$ | | 96.5 | 88.3 | 6.3 | 5.4 | 0 | 5.30 | 1.77 |
| HS-Co/$CeO_2$ | 12/1 | 97.1 | 91.6 | 3.9 | 4.5 | 0 | 5.49 | 1.83 |
| HS-KCo/$CeO_2$ | | 97.7 | 92.7 | 3.7 | 3.6 | 0 | 5.56 | 1.85 |

On the contrary, the selectivities of carbon-containing gaseous products show striking difference among the catalysts. Comparison of the LS- and HS-catalysts shows that the HS is more selective towards $CO_2$ (and less to CO) than the LS-counterpart for all $H_2O$/EtOH molar ratios. At the 3/1 molar molar ratio both LS- and HS-catalysts have lower $CO_2$ and higher CO and $CH_4$ selectivities than the HS-K, though more $CH_4$ is observed for the HS- as compared to LS-catalyst. In the excess of water, the increase of $CO_2$ selectivity over the LS- and HS-catalysts is accompanied with a decrease of CO and $CH_4$ formation. The results also show that in the case of the HS-K the influence of the $H_2O$/EtOH molar ratio on the catalyst's selectivity in the ESR is negligible.

*1.5. The influence of the ESR conditions on the catalysts' coking*

Presence of big cobalt particles in the HS-catalyst is expected to make it more vulnerable to coking than its LS-counterpart [117, 118]. The XPS spectra obtained at the 3/1 molar ratio are in agreement with this hypothesis, but in the excess of water, less carbon was observed on LS-catalyst after 1 h ESR (Fig. 2-4 and Table 2). The different kinetics of carbon deposition might account for this behaviour in this two cases. More information about the kinetics of carbon deposition under long ESR reaction periods is provided by gravimetric studies (Fig. 5). It's important to keep in mind the substantial differences in the catalytic reactors, allowing only certain trends to be taken into account. Nevertheless, based on the XPS results the oxidation state of the catalysts was not dramatically different, therefore, the weight changes can be primarily assigned to coke deposition.

In general, the weight change of the unpromoted catalysts (LS and HS) is significantly higher as compared to the HS-K catalyst, confirming that potassium inhibits carbon formation and catalyst's oxidation, in accordance with the XPS results.

Under the stoichiometric (3/1 mol/mol) reaction mixture the weight of the LS-catalyst has increased sharply to reach an almost constant value, while in the case of the HS-catalyst the weight gain was slower.

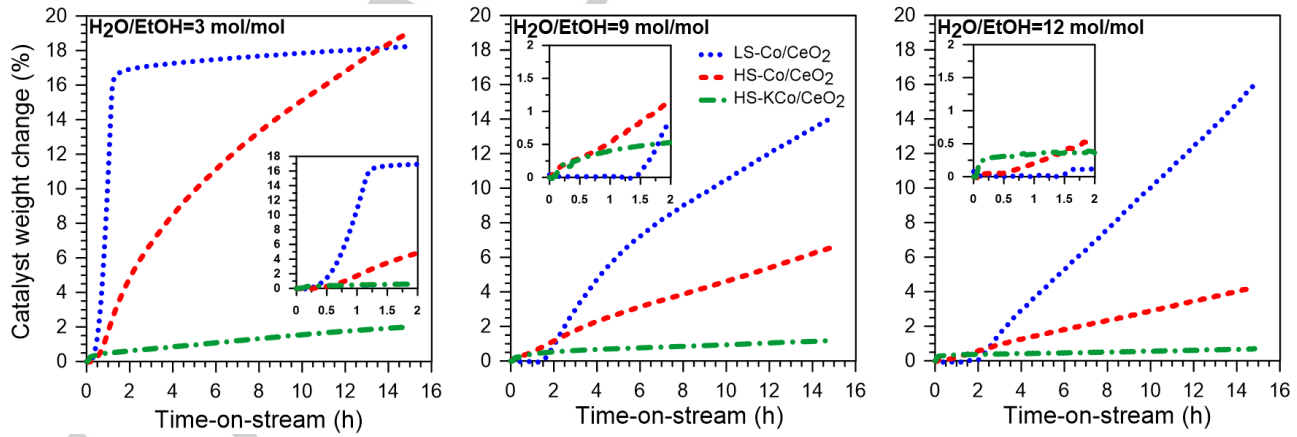


**Figure 5.** The gravimetric results for the LS-Co/$CeO_2$ (···), HS-Co/$CeO_2$ (---) and HS-KCo/$CeO_2$ (– · –) catalysts under the $H_2O$/EtOH = 3/1, 9/1 and 12/1 mol/mol.

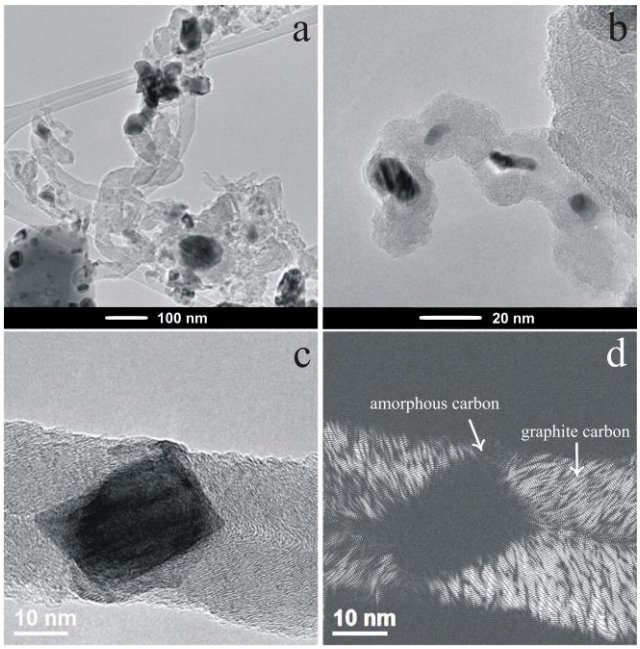


**Figure 6.** TEM images of the LS-Co/$CeO_2$ catalyst after 1 h ESR (T = 420°C, $H_2O$/EtOH = 3/1 mol/mol).

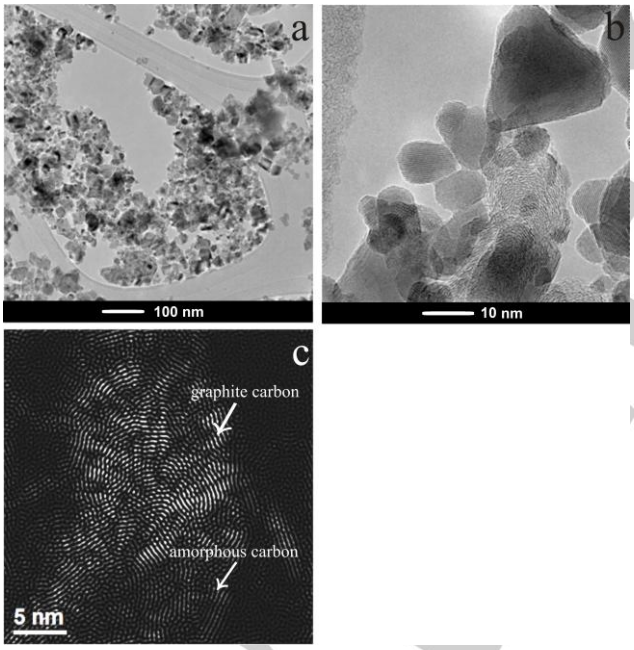


**Figure 7.** TEM images of the HS-Co/$CeO_2$ catalyst after 1 h ESR (T = 420°C, $H_2O$/EtOH = 3/1 mol/mol).

However, note that the weight gain for both catalysts starts immediately after exposure to the ESR reactants (see insets of Fig. 5). On the other hand, at reactants mixtures rich in water the weight gain does not start simultaneously for the LS- and HS-catalysts. In particular carbon deposition (and oxidation) on the LS-catalyst necessitates an induction period of 1 to 2 hours but after that increases rapidly and finally the catalyst is the most intensively coked. Conversely, catalyst's oxidation and carbon deposition on the HS-catalyst starts immediately and occurs gradually but with lower rate as compared to the LS-catalyst.

The explanation of the differences at the carbon deposition kinetics between the catalysts is out of the scope of this paper. However, from Fig. 5 (insets) it is evident that during the reaction period used at XPS experiments (1 hour) carbon deposition for the LS-catalyst at water rich ESR mixtures is limited, in agreement with our the XPS studies.

The morphology of the spent catalysts after 1 h ESR reaction under the 3/1 molar ratio was studied by TEM, with emphasis on the carbon deposit formed during the ESR (Fig. 6-8). The TEM analysis of spent LS- and HS-samples revealed mainly graphitic carbon, although amorphous carbon was also detected, but to a lower extent. However, the morphology of carbon deposits differs among the catalysts. On the LS (Fig. 6) mostly carbon filaments in which encapsulated cobalt particles could be seen. Carbonaceous deposit detected on the surface of HS-catalyst looks more like a few atomic layers of carbon, mostly located at the boundary of cobalt and ceria crystallites, indicating that reaction occurs in this direction at the Co–$CeO_x$ interface (Fig. 7). On the TEM images of the HS-K negligible amounts of carbon were found (Fig. 8), in accordance with the XPS results.

It can be concluded that the form of the carbon deposit depends on the support morphology and cobalt particles size. The catalyst with larger cobalt particles favours the growth of carbon nanofibers [118]. Basing on the XPS results, the surface amount of coke on both LS- and HS-catalysts is almost comparable after 1 h ESR for the $H_2O$/EtOH = 3/1 mol/mol. TEM studies have shown that significantly less bulk carbon was found

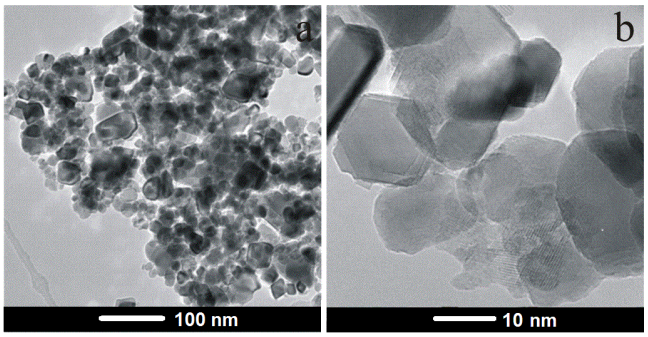


**Figure 8.** TEM images of the HS-KCo/$CeO_2$ catalyst after 1 h ESR (T = 420°C, $H_2O$/EtOH = 3/1 mol/mol).

in the case of the HS-catalyst, being compatible with results of gravimetric measurements (Fig. 5). TEM images prove that in the case of the low surface area catalyst, carbon diffused inside cobalt crystallites, destroying the sample from the inner layers and it is deposited mainly in the whiskers form, while on the high surface counterpart, carbon was deposited gradually only the outer layers of catalysts.

## Discussion

### *2.1. The influence of the $H_2O$/EtOH molar ratio on the catalysts' surface*

Fig. 9 shows how the reactants composition influences the catalysts' surface state. The degree of catalysts' surface reorganization under conditions of the steam reforming of ethanol can be attributed to difference in the $H_2O$/EtOH molar ratio. Our results prove that higher dispersion (smaller crystallites) of both ceria support and cobalt in the unpromoted catalysts makes its oxidation easier under ESR conditions – this catalyst was also more resistant to reduction, as it is shown in Fig. 1. The ceria support in the unpromoted catalysts is progressively oxidized (Fig. 9a) with increasing excess of water. Ceria with the higher surface area (smaller ceria crystallites) is oxidized to a larger extent (on its surface the concentration of Ce(III) ions is lower) than that of the low-surface area. Moreover, the water excess facilitates oxidation of cobalt (Fig. 9b). As in the case of ceria, the more intensive oxidation of cobalt (the larger Co(II)/(Co(0)+Co(II)) atomic ratio) occurs when the small cobalt crystallites were deposited on the high-surface area ceria support. The result is consistent with literature conclusions that supported small cobalt crystallites tend to get oxidized more readily than the larger ones [8, 36, 40, 43, 53].

The increased $H_2O$/EtOH molar ratio in the reaction mixture also promotes increasing hydroxyl's species concentration (Fig. 9c) on the catalyst's surface (the hydroxyls' concentration is considered on the whole surface of catalysts basis, as the XPS data do not enable to differentiate location of hydroxyls, on cobalt or on ceria). Additionally so far published papers suggest that at temperatures of 350–450ºC the formation of OH species, due to dissociation of water, is favourable on the surface of both ceria and cobalt [8, 27, 56, 57, 109, 119]. In spite of very similar, low concentration of hydroxyls under the 3/1 $H_2O$/EtOH molar ratio on the surface of potassium-free catalysts (Fig. 9), the increasing water extent increases the difference between abundance of these species on the surface of the unpromoted catalysts. Fig. 9 shows that higher concentration of hydroxyls exists on the surface of the LS-catalyst. The higher abundance of hydroxyls might be related to lower oxidation of both main components of the LS-catalyst – the higher share of metallic, not oxidized cobalt in the active phase or/and the higher concentration of surface Ce(III) ions in the ceria support – the larger surface concentration of hydroxyls.

In contrast to the unpromoted HS-catalyst, the ceria support in the potassium-promoted HS-K catalyst is already more reduced under the lowest, stoichiometric reactants ratio and it shows further reduction of cerium surface ions with the increase

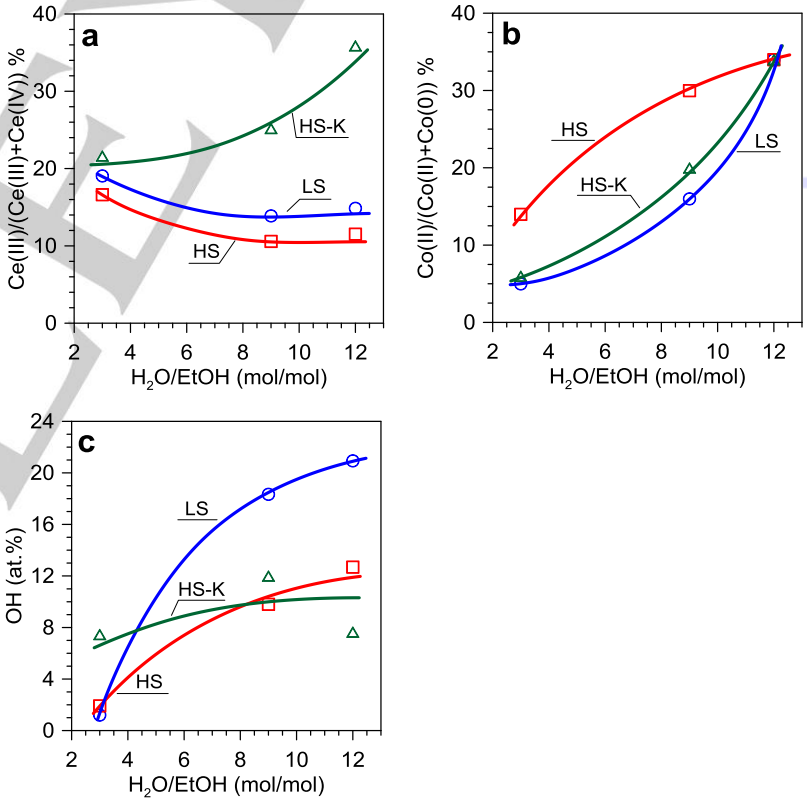


**Figure 9.** Dependence of percentage concentration of (a) Ce(III)/(Ce(III)+Ce(IV)), (b) Co(II)/(Co(II)+Co(0)) and (c) adsorbed hydroxyls with the $H_2O$/EtOH molar ratio for the LS-Co/$CeO_2$, HS-Co/$CeO_2$ and HS-KCo/$CeO_2$ catalysts in the ESR at 420°C.

of the water excess in the reaction mixture (Fig. 9a). At the same time, the cobalt active phase also stays in less oxidized form as compared to the unpromoted HS-catalyst (Fig. 9b) – the extent of its oxidation is similar to one of the LS-catalyst. The concentration of surface hydroxyls is much higher already under the 3/1 $H_2O$/EtOH molar ratio than this on the unpromoted HS-catalyst and it changes only a little with the $H_2O$/EtOH molar ratio (Fig. 9c). Under higher water vapour excess this difference disappears. Undoubtedly, all these differences in the state of the catalyst's surface, seen between unpromoted HS- and promoted HS-K catalysts, result from the additional presence of potassium on the catalyst's surface, which concentration of which also changes with the reactants molar ratio (Table 2). The progressive increase of the total concentration of potassium on the catalyst's surface simultaneously with the excess of water vapour in the reaction mixture results probably from the re-dispersion of potassium-containing aggregates, caused by increased amount of chemisorbed and dissociated water vapour. As in the case of hydroxyls, the concentration of potassium-containing sites is considered here on the whole surface of catalysts basis, without distinction between their location, on cobalt or on ceria. It was shown in ref. [31] that potassium on a very similar and free of coke catalyst is well distributed on the whole catalyst's surface.

### *2.2. Correlation of the ESR catalytic performance with the catalysts' surface state*

Considering the influence of the chemical state of the surface of different ceria-supported cobalt catalysts on the course of the steam reforming of ethanol, the correlations of the selectivity towards carbon dioxide formation with the oxidation state of cobalt active phase and its support were drawn (Figs. 10a and 10b). Taking into account the unpromoted catalysts only, one might suppose that cobalt oxidation state can be an important factor influencing the ESR selectivity (Figs. 10a). However, the performance of the potassium-promoted HS-K catalyst prevents drawing such general conclusion; the same oxidation degree of cobalt in the HS and HS-K catalysts enables obtaining very different carbon dioxide production. It proves that potassium introduces other selective and active sites responsible for the ESR – oxidation of cobalt has no response in carbon dioxide formation. The same conclusion can be drawn when considering the role of the oxidation state of the ceria support. Both correlations shown in Figs. 10a and 10b lead us to the assertion that oxidation-reduction of these main catalysts' components is not a general factor, crucial for the selective transformations of ethanol. The presence of oxidized cobalt and reduction-oxidation of the ceria support are unavoidable effects, dependent on the $H_2O$/EtOH molar ratio; however, not involved directly in making the catalyst's selective for the ESR. However, it was shown in ref. [33] that they might be important in the first step of the ESR, i.e., in oxidative dehydrogenation of alcohol and ethoxide species formation.

An important feature of the catalysts' surface, influencing selectivity of the ESR would be the concentration of hydroxyl species. In Fig. 10c one can see straight-linear relationships of concentration of surface adsorbed hydroxyls over LS-, HS- and HS-K catalysts with the selectivity of carbon dioxide formation. The low-dispersed LS-catalyst requires larger concentration of surface adsorbed hydroxyl species than the very well-dispersed HS to achieve the same selectivity of the ESR – this difference we will discuss in next paragraphs. However, before the $CO_2$ selectivity over the HS-catalyst gains on that characteristic of the potassium-promoted HS-K-catalyst (i.e., in the lower range of OH concentration), the same abundance of hydroxyl species leads to different selectivity over those two catalysts. Similar picture is seen in relationships of the OH concentration and selectivities towards remaining ESR products, i.e., hydrogen, carbon monoxide and methane (see Fig. S5 in Supplementary Information). It suggests the existence of additional selective sites on the surface of promoted catalyst, related to the presence of potassium promoter on the catalyst's surface, i.e., K–O sites. These potassium-containing sites (K–O) are expected to play a promoting role in the steam reforming of ethanol, providing an additional oxygen-containing species reservoir. Similar suggestion that potassium encourages formation of active oxygen species, which are very important intermediates for soot combustion, was given by M. Sun et al. [94]. Taking both, OH species and K–O sites, into consideration the selectivities of the ESR to all products over HS- and HS-K catalysts form coherent dependences, with limits characteristic for the HS- catalyst (Figs. 11a-11c). Those limits are consistent with the thermodynamic limit of the hydrogen yield in the ethanol steam reforming; considering equilibrium states of side reactions the equilibrium hydrogen yield of 5.56 mole per one mole of ethanol in the feed are obtainable as against the stoichiometric value of 6.0 [67]. Also, for the same reason the thermodynamic yield of carbon dioxide is lower than the stoichiometric value of

2.0. The yields of produced hydrogen and carbon dioxide in our studies reach the thermodynamic values (Fig. 11e). In the feed with the $H_2O$/EtOH molar ratio higher than stoichiometric value of 3/1 the total concentration of OH species and K–O sites on the surface of potassium-promoted catalyst is even larger than necessary for the selective course of the ESR to gaseous products. However, a higher concentration of OH species and K–O sites is required for hindering of coke deposition on the catalysts, including all coke forms and all catalysts studied in this work (Fig. 11f). Small concentration of OH species and K–O sites leads to dramatic coking of the catalysts, with formation of completely (or almost completely) dehydrogenated C=C type carbonaceous deposit, in a large part as graphitic whiskers and layers (see Table S1 in Supplementary Information and Figs. 6-8). An increasing of those selective-acting surface sites first of all significantly lowers the amount of coke deposited and also changes its type from more dehydrogenated to $CH_x$ type. For total elimination of coking phenomena, the high abundance of OH species and K–O sites, equal to or large than 25 at.% of the whole surface of catalyst is required.

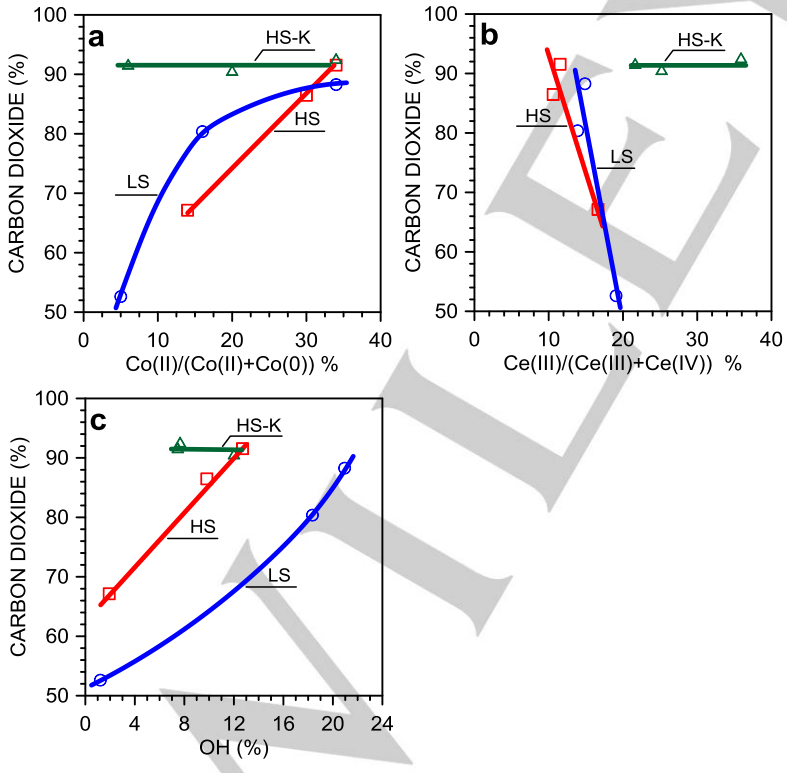


**Figure 10.** Correlation of $CO_2$ selectivity for the LS-Co/$CeO_2$, HS-Co/$CeO_2$ and HS-KCo/$CeO_2$ catalysts under the ESR at 420°C with percentage concentration of (a) Ce(III)/(Ce(III)+Ce(IV)), (b) Co(II)/(Co(II)+Co(0)), and (c) adsorbed hydroxyls on the surface. Each point represents the different $H_2O$/EtOH molar ratio.

Among surface oxygen-containing species molecular water is also present. However, physically adsorbed water molecules cannot form transition activated complexes, required in a catalytic reaction, on the surface of heterogeneous catalyst. Therefore, water species can be considered merely as spectators, excluded from direct participation in the ESR over catalyst's surface. The selectivity of the steam reforming of ethanol does not depend solely on the population of OH species on the catalyst's surface since the LS-catalyst is less selective towards all products despite the fact that it has more hydroxyls adsorbed than the HS-catalyst (Figs. 11a–11d). It suggests that the catalyst's morphology and location where oxygen-containing species are adsorbed may be equally important as their abundance. The difference in the ESR selectivity is related to the dispersion of both catalysts. The size of cobalt crystallites is very different: 3.8 nm in more selective HS-catalyst and 39.3 nm in the less selective LS. Whereas the size of ceria support crystallites is 25.6 nm and 87.1 nm, for HS and LS respectively. The well dispersed, small crystallites usually have more low-coordinated sites (corners, edges and another defects on the surface of crystal lattice like steps, adatoms), which are the best and the strongest sites for chemisorption and dissociation of various chemical molecules, including also water (and ethanol) molecules. On the other hand, a close contact of both catalyst's components and a short-enough distance from their border to the middle of the cobalt crystallites surface (where the number of low-coordinated sites is lower than near crystallite edge) [1] also may have a significant selective influence on the effects of the ESR [8] – reagents and their intermediates chemisorbed on the cobalt and on the ceria support may interact together to form desirable products of the ESR, i.e., hydrogen and carbon dioxide. When the surface distance from the cobalt-ceria support border is too long (as in the case of a center of large crystallites in the LS-catalyst), nonselective ethanol transformations may take place, without the possibility of by-products to react with activated water. Due to an insufficient surface concentration of hydroxyl species acetaldehyde remains among final products (Fig. 11d). The comparison of the ESR effects over HS- and LS-catalysts leads us to the suggestion

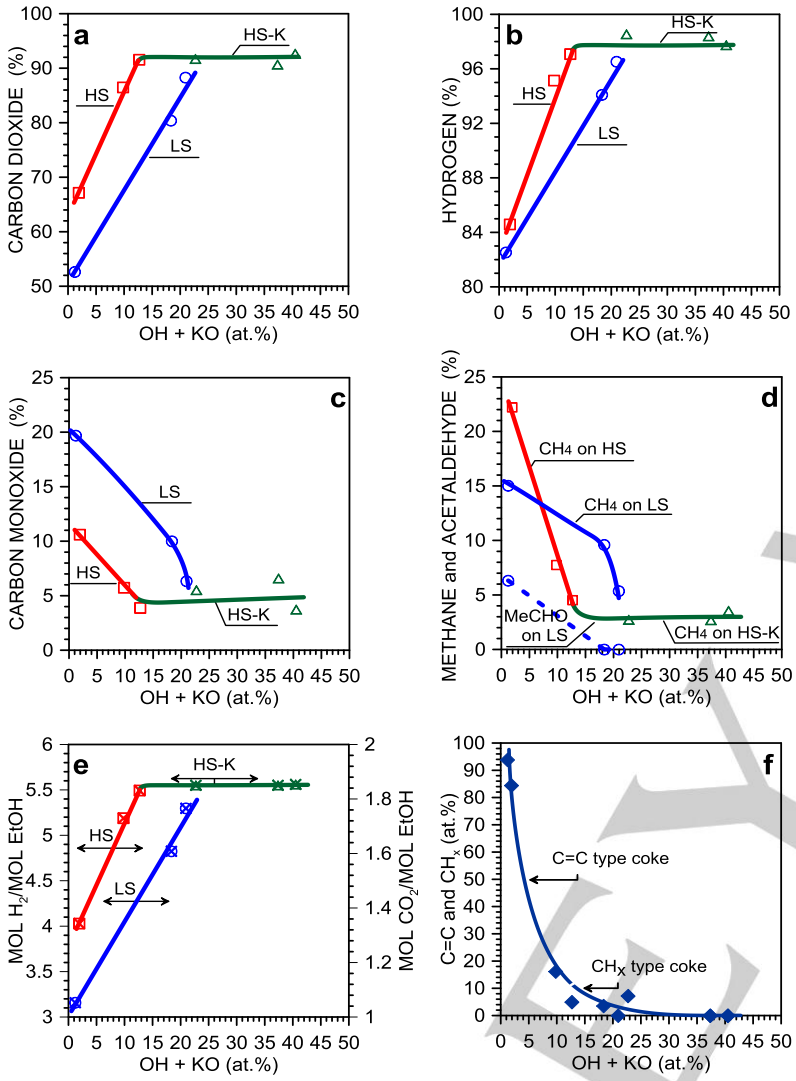


**Figure 11.** Correlation of (a-d) the catalysts' selectivity towards $H_2$ and carbon-containing product, (e) $H_2$ and $CO_2$ yield, and (f) the concentration of C=C and $CH_x$ species on the whole surface, with the concentration of oxygen-containing species on the surface of the LS-Co/$CeO_2$, HS-Co/$CeO_2$ and HS-KCo/$CeO_2$ catalysts in the ESR at 420°C.

that the selective ceria-supported cobalt catalyst should have well dispersed cobalt particles deposited on the well dispersed support, which is in agreement with previously published results [3, 13, 21].

## Conclusions

The chemical surface state and the catalytic performance of cobalt catalysts with micro- and nano-dispersed ceria supports were investigated under the steam reforming of ethanol at 420°C for the $H_2O$/EtOH molar ratios equal to 3/1, 9/1 and 12/1. In the case of the nano-catalyst the effect of potassium promotion was also examined.

We found that the reduction degree of cobalt oxide and ceria during activation of catalysts with hydrogen depends on ceria's support dispersion. Cobalt oxide supported on low-dispersed ceria is more vulnerable to reduction than its counterpart with high-dispersed ceria, while potassium promoter facilitates reduction of cobalt oxide. The ceria support is reduced to some extent only in the low-dispersed catalyst, while in the unpromoted and potassium-promoted catalysts with high-dispersed ceria it remains practically fully oxidized after pre-reduction.

The catalysts' surface undergoes reorganization under conditions of the steam reforming of ethanol to a degree dependent on the $H_2O$/EtOH molar ratio. We proved that higher dispersion (smaller crystallites) of both ceria support and cobalt in the unpromoted catalyst makes its oxidation easier under ESR conditions. The water excess in the ethanol-water vapours feed facilitates oxidation of both catalyst's components. In contrast to the unpromoted high-dispersed catalyst, the ceria support in the potassium-promoted catalyst is more reduced even under the lowest, stoichiometric reactants ratio and it undergoes further reduction with the increase of the water excess in the reaction mixture. In the potassium-promoted catalyst the cobalt active phase exists mainly in metallic form, similarly to the unpromoted catalysts.

We proved that oxidation-reduction of the main catalysts' components is not a general factor crucial for the selective transformations of ethanol. The presence of oxidized cobalt and reduction-oxidation of the ceria support are unavoidable effects, dependent on the $H_2O$/EtOH molar ratio; however, not involved directly in doing the catalyst selective for the ESR.

The concentration of potassium promoting sites ($K^{\delta+}$–$O^{\delta-}$ sites) on the catalyst's surface progressively increases simultaneously with the excess of water vapour in the reaction mixture. These sites may play promoting role in the steam reforming of ethanol, providing an additional oxygen-containing species reservoir.

The most crucial for selective conversion of ethanol over unpromoted catalysts is concentration of hydroxyl species on the catalysts surface, which increases with increased $H_2O$/EtOH molar ratio in the reaction mixture in the extent depending on the dispersion of catalysts components. In the case of promotion of the catalyst with potassium, the increasing hydroxyl concentration is supplemented by $K^{\delta+}$–$O^{\delta-}$ sites. We found good, coherent relationship of OH species along with $K^{\delta+}$–$O^{\delta-}$ sites, and the selectivity of the ESR to all gaseous products over unpromoted and promoted catalysts, with limits consistent with the thermodynamic limit of the hydrogen yield. Beside surface concentration of hydroxyl species, the catalyst's morphology and location where oxygen-containing species are chemisorbed may be equally important to their abundance – the selective ceria-supported cobalt catalyst should have well dispersed cobalt particles deposited on the well dispersed support.

Beside the role played by oxygen-containing species in improving catalytic performance of catalysts, the increasing presence of both OH and $K^{\delta+}$–$O^{\delta-}$ sites was found to lower the amount of coke deposited as well as to change its type from fully dehydrogenated C=C to $CH_x$ type. For total elimination of coking phenomena higher abundance of OH species and $K^{\delta+}$–$O^{\delta-}$ sites on the catalyst's surface than that necessary for the selective ESR to gaseous products is required.

## Experimental Section

*Catalysts preparation*

The $Co/CeO_2$ catalysts were prepared by impregnation of the commercial nano- (HS) and micro- (LS) dispersed ceria support (<25 nm and <5 μm, respectively, Aldrich) [13]. Prior to impregnation, the supports were dried at 110°C for 3 h. The solution of cobalt nitrate and citric acid CA (the relative molar concentration of Co and CA was 1/1) was used for impregnation. After the impregnation, the catalysts' precursor were dried at 110°C for 12 h, then calcined at 400°C with a heating rate of 2°C/min up to the calcination set point and maintained for 1 h at this temperature [60, 73]. The catalysts were denoted as LS- and HS-$Co/CeO_2$. Next, the part of obtained HS-$Co/CeO_2$ catalyst's precursor was impregnated with potassium nitrate solution in order to introduce 2 wt.% of potassium promoter to the catalyst [31, 60] (further abbreviated as HS-K) and again it was dried at 110°C for 12 h, then calcined at 400°C with a heating rate of 2°C/min up to the calcination set point and maintained for 1 h at this temperature.

*Catalysts characterization*

X-ray fluorescence technique (XRF) was used to determine the bulk cobalt content in the catalyst. The measurements were performed by Axios$^{mAX}$ (PANalytical) spectrometer fitted with a Rh (4 kW) tube. The SuperQ 5 software package was used for spectral deconvolution and for the calculation of the component contents. The quantification was based on the external synthetic standard.

The X-ray powder diffraction patterns of the supports and catalysts were recorded using an Empyrean X-ray (PANalytical) diffractometer equipped with a PIXcel$^{3D}$ detector using Cu Kα radiation (λ = 0.154 nm). Data were acquired from 10 to 110º(2θ) with a 0.026º(2θ) step size. The measured patterns were compared with the International Centre for Diffraction Data (ICDD) PDF-4+ database for phase identification and the crystallite size was calculated using the Scherrer equation. A correction for instrumental broadening was applied using a reference standard ($LaB_6$).

The porosity and BET total surface area of catalysts were measured by the low temperature (-196°C) nitrogen adsorption in the ASAP 2420 (Micromeritics) analyzer after degassing the samples at 200°C. The average pore diameter and the volume of pores were calculated from desorption data using Barret-Joyner-Halenda (BJH) method.

The active metal surface area, dispersion and mean cobalt particles size of catalysts pre-reduced *in situ* in hydrogen at 420°C (1 h), were calculated from hydrogen chemisorption data obtained at an ASAP 2020 (Micromeritics) analyzer at 130°C [120]. The H/Co stoichiometry of 1/1 and the spherical shape of cobalt particles were used for calculation of the mean size. The detailed description of the calculation method has been given elsewhere [120].

The gravimetric studies of catalysts' coking in the ESR were carried out in TG121 microbalance system (CAHN), under dynamic conditions in a quartz reactor with a continuous flow of $H_2O$/EtOH vapours diluted with He (He 50 $cm^3$/min + 3 $cm^3$/min mixture) at 420°C for 21 hours. The molar ratio of $H_2O$/EtOH was equal 3/1, 9/1 and 12/1. Prior to the reaction, catalysts (0.05 g of the catalyst (0.15–0.3 mm)) were reduced by passing 10% $H_2$/He flow (70 $cm^3$/min) at the temperature of 420°C for 1

hour (the linear temperature increase to 420°C was 10°C/min). In all studies 96% bio-EtOH was used for the reaction mixture preparation.

*Combined XPS and catalytic performance experiments*

X-ray Photoelectron Spectroscopy (XPS) studies were performed in a multi-chamber UHV system (PREVAC, Poland) equipped with a monochromatized Al source (XM 650 X Ray Monochromator) source operating at 360 W and a hemispherical electron analyzer (Scienta R4000). The pass energy of the analyser was set at 200 eV (energy step 0.5 eV) for survey scan and 50 eV (energy step 0.1 eV) for high resolution Co 2p, Ce 3d, O 1s, C 1s, Ce 4s and K 2p spectra. The base pressure in the analysis chamber was $5 \cdot 10^{-8}$ mbar. Data processing was performed with the CasaXPS software (v 2.3.16 PR 1.6), taking into account the relative sensitivity factors (provided by CasaXPS software) for Co $2p_{3/2}$, Ce 3d, O 1s, C 1s, K 2p regions. After Shirley background subtraction the Co 2p and Ce 3d regions were fitted using spectra recorded over reference samples. The quantification of the Co 2p and Ce 3d regions was performed by the fitting procedure based on the linear combination of two reference spectra. The percentage contribution of Ce(III) and Co(II) were calculated using the peak areas emerged by the linear fitting procedure of references according to the formulas $\mathrm{Ce(III)} = \frac{\mathrm{Ce(III)}}{\mathrm{Ce(III)} + \mathrm{Ce(IV)}} \cdot 100\%$ and $\mathrm{Co(II)} = \frac{\mathrm{Co(II)}}{\mathrm{Co(II)} + \mathrm{Co(0)}} \cdot 100\%$.

Catalytic tests were performed in a high pressure flow reactor connected through the radial distribution chamber with the analysis chamber. The samples were pressed into 10 mm diameter pellets and attached on a dedicated sample holder (PTS HPC RES/C-K RG). The temperature of the sample was measured with a thermocouple in contact with the sample holder and regulated by HEAT2-PS power supply. Prior to the reduction samples were heated in a load lock chamber by halogen lamp for 1.5 h to remove volatile surface adsorbed impurities. The reduction was carried out in the flow reactor at 420°C for 1 h, by hydrogen diluted in argon (50/50 $cm^3$/min, p = 1 atm). The samples were cooled down to 200°C in the flow of $H_2$/Ar and then the flow of hydrogen was stopped. Further cooling down (to 80°C) was in the flow of Ar only. Before the reaction, samples were heated in the flow of Ar (50 $cm^3$/min, p = 1 atm) with the ramp rate 10°C/min. The water/ethanol vapours (3 $cm^3$/min, $p_{partial}$ = 57 mbar) diluted in Ar (50 $cm^3$/min) were introduced to the reactor (by heated lines) at the reaction temperature (420°C) by a Controlled Evaporation and Mixing (CEM) System (Bronkhorst). The total pressure in the reactor during the reaction was equal 1 atm. The ESR was carried out over 1 h, next the flow of vapours was stopped and samples were quenched in the flow of Ar till 80°C and transferred to the XPS analysis chamber.

In the course of the ESR reaction, carried out in the high pressure cell, the composition of gas phase products ($H_2$, $CO_2$, CO, $CH_4$) was monitored *on-line* by means of a micro-GC (Agilent, 490-GC).

*Catalytic tests in a fixed-bed reactor*

Since the micro-GC does not allow to analyse the liquids such as: ethanol, water, and acetaldehyde, in order to gain a better insight into catalytic properties of the examined catalysts, the ESR reaction ($H_2O$/EtOH molar rations 3/1, 9/1 and 12/1) was carried out also in a fixed-bed continuous-flow quartz reactor (Microactivity Reference unit, PID Eng & Tech.) under atmospheric pressure. The pre-treatment and reaction conditions were kept identical to those described above for reactor attached to the UHV setup (the same amount of pressed in pellet catalyst, the same reduction procedure and the flow of reactants). The analysis of the reaction mixture and the reaction products (all in the gas phase) were carried out *on-line* by means of two gas chromatographs. One of them, Bruker 450-GC was equipped with two columns, the first filled with a porous polymer Porapak Q (for all organics, $CO_2$ and $H_2O$ vapour) and the other one – capillary column CP-Molsieve 5Å (for $CH_4$ and CO analysis). Helium was used as a carrier gas and a TCD detector was employed. The hydrogen concentration was analyzed by the second gas chromatograph, Bruker 430-GC, using a Molsieve 5Å column, argon as a carrier gas and a TCD detector.

The total conversion of ethanol ( $X_{EtOH}$ ), water ( $X_{H_2O}$ ) and conversions of ethanol into individual carbon-containing products ( $X_{CP}$ ) were calculated from their concentrations before and after the reaction, taking into account changes in the gas volume during the reaction, from the equations:

$$X_{EtOH} = \frac{C_{EtOH}^{in} - C_{EtOH}^{out} \cdot K}{C_{EtOH}^{in}} \cdot 100\%$$

,

$$X_{H_2O} = \frac{C^{in}_{H_2O} - C^{out}_{H_2O} \cdot K}{C^{in}_{H_2O}} \cdot 100\%$$ ,

$$X_{CP} = \frac{C^{out}_{CP} \cdot K}{n/2 \cdot C^{in}_{EtOH}} \cdot 100\%$$

where:

$C^{in}_{EtOH}$ and $C^{in}_{H_2O}$ – is the molar concentration of EtOH and $H_2O$ in the reaction mixture (mol%); $C^{out}_{EtOH}$ and $C^{out}_{H_2O}$ – is the molar concentration of EtOH and $H_2O$ in the post-reaction mixture (mol%); $C^{out}_{CP}$ – is the molar concentration of carbon-containing products in the post-reaction mixture (mol%); n – is number of carbon atoms in carbon-containing molecule of the reaction product; K – is the volume contraction factor ($K = C^{in}_C / C^{out}_C$ where $C^{in}_C$ and $C^{out}_C$ are the molar concentrations of carbon in the ethanol feed to the reaction and in all carbon-containing compounds which were present in post reaction gases, respectively). The selectivity of ethanol conversion into individual carbon-containing gaseous and liquid products was expressed as $(X_{CP}/X_{EtOH}) \cdot 100\%$.

The selectivity of hydrogen formation was determined as:

$$H_2 \text{ selectivity} = \frac{C^{out}_{H_2}}{C^{out}_{H_2} + 2 \cdot C^{out}_{CH_4} + 2 \cdot C^{out}_{CH_3CHO}} \cdot 100\%$$

where:

$C^{out}$ – is the molar concentration of the hydrogen-containing products in the post-reaction mixture (mol%). Hydrogen, methane and acetaldehyde were the only hydrogen-containing products of the ESR.

*Post-reaction TEM catalysts' characterization*

The spent catalysts (after 1 h of the ESR) were grinded to a fine powder in an agate mortar and then mixed with 99.8% ethanol into the ultrasonic homogenizer for 20 s. The slurry containing the catalyst was pipetted on a 200 mesh copper grid covered with lacey formvar and stabilized with carbon (Ted Pella Company) and left on a filter paper to evaporate ethanol. Subsequently, the sample deposited on the grid was inserted to the sample holder and transferred to the electron microscope. The images were recorded in a transmission electron microscope (Tecnai $G^2$ 20 X-TWIN FEI Company), equipped with $LaB_6$ emitter and using 200 kV electron beam accelerating voltage [35].

## Acknowledgements

S.T. would like to thank for the financial support from French Government, Campus France, UdS (France) and UMCS (Poland). The research was carried out with the equipment purchased thanks to the financial support of the European Regional Development Fund in the framework of the Polish Innovation Economy Operational Program (contract no. POIG.02.01.00-06-024/09 Center of Functional Nanomaterials; www.cnf.umcs.lublin.pl).

**Keywords:** ethanol steam reforming • cobalt-based catalysts • ceria support • potassium promoter • XPS

[1] D. Zanchet, J.B.O. Santos, S. Damyanova, J.M.R. Gallo, J.M.C. Bueno, *ASC Catal.* **2015**, *5*, 3841–3863.

[2] B. Bayram, I.I. Soykal, D. von Deak, J.T. Miller, U.S. Ozkan, *J. Catal.* **2011**, *284*, 77–89.

[3] I.I. Soykal, H. Song, U.S. Ozkan, *ACS Catal.* **2012**, *2*, 2335–2348.

[4] A.M. Karim, Y. Su, M.H. Engelhard, D.L. King, Y. Wang, *ACS Catal.* **2011**, *1*, 279–286.

[5] A.R. Passos, L. Martins, S.H. Pulcinellin, C.V. Santilli, V. Briois, *Catal. Today* **2014**, *229*, 88–94.

[6] M.N. Barroso, M.F. Gomez, L.A. Arru, M.C. Abello, *Reac. Kinet. Mech. Cat.* **2015**, *115*, 535–546.

[7] E. Varga, Z. Ferencz, A. Oszkó, A. Erdöhelyi, J. Kiss, *J. Mol. Catal. A* **2015**, *397*, 127–133.

[8] H. Sohn, I.I. Soykal, S. Zhang, J. Shan. F. Tao, J.T. Miller, U.S. Ozkan, *J. Phys. Chem. C* **2016**, *120*, 14631–14642.

[9] H. Song, L. Zhang, U.S. Ozkan, *Top. Catal.* **2012**, *55*, 1324–1331.

[10] Zs. Ferencz, A. Erdőhelyi, K. Baan, A. Oszkó, L. Óvári, Z. Kónya, C. Papp, H.-P. Steinrück, J. Kiss, *ACS Catal.* **2014**, *4*, 1205–1218.

[11] I.I. Soykal, B. Bayram, H. Sohn, P. Gawade, J.T. Miller, U.S. Ozkan, *Appl. Catal., A* **2012**, *449*, 47–58.

[12] H. Wang, L. Zhang, M. Li, Y. Liu, X. Bai, *J. Rare Earth* **2013**, *31*, 565–571.

[13] A. Machocki, A. Denis, W. Grzegorczyk, W. Gac, *Appl. Surf. Sci.* **2010**, *256*, 5551–5558.

[14] S.-W. Yu, H.-H. Huang, C.-W. Tang, C.-B Wang, *Int. J. Hydrogen Energy* **2014**, *39*, 20700–20711.

[15] H. Song, U.S. Ozkan, *J. Catal.* **2009**, *261*, 66–74.

[16] H. Sohn, U.S. Ozkan, *Energy Fuel* **2016**, *30*, 5309-5322.

[17] J. Llorca, P.R. de la Piscina, J.A. Dalmon, N. Homs, *Chem. Mater.* **2004**, *16*, 3573–3578.

[18] S. Tuti, F. Pepe, *Catal. Lett.* **2008**, *122*, 196–203.

[19] M.P. Hyman, J.M. Vohs, *Surf. Sci.* **2011**, *605*, 383–389.

[20] N. Laosiripojana, S. Assabumrungrat, *Appl. Catal., B* **2006**, *66*, 29–39.

[21] I.I. Soykal, H. Sohn, D. Singh, J.T. Miller, U.S. Ozkan, *ASC Catal.* **2014**, *4*, 585–592.

[22] M. Greluk, P. Rybak, G. Słowik, M. Rotko, A. Machocki, *Catal. Today* **2015**, *242*, 50–59.

[23] S. Ogo, T. Shimizu, Y. Nakazawa, K. Mukawa, D. Mukai, Y. Sekine, *Appl. Catal., A* **2015**, *495*, 30–38.

[23] B. Banach, A. Machocki, *Appl. Catal., A* **2015**, *505*, 173–182.

[25] S. Turczyniak, W. Luo, V. Papaefthimiou, N. S. Ramgir, M. Haevecker, A. Machocki, S. Zafeiratos, *Top. Catal.* **2016**, *59*, 532–542.

[26] V.M. Lebarbier, A.M. Karim, M.H. Engelhard, Y. Wu, B.-Q. Xu, E.J. Petersen, A.K. Datye, Y. Wang, *ChemSusChem* **2011**, *4*, 1679–1684.

[27] I.I. Soykal, H. Song, J.T. Miller, U.S. Ozkan, *Top Catal.* **2014**, *57*, 785–795.

[28] J. Llorca, J.-A. Dalmon, P.R. de la Piscina, N. Homs, *Appl. Catal., A* **2003**, *243*, 261–269.

[29] S. Turczyniak, D. Teschner, A. Machocki, S. Zafeiratos, *J. Catal*. **2016**, *340*, 321–330.

[30] J. Sun, A.M. Karim, D. Mei, M. Engelhard, X. Bao, Y. Wang, *Appl. Catal., B* **2015**, *162*, 141–148.

[31] G. Słowik, M. Greluk, A. Machocki, *Mater. Chem. Phys.* **2016**, *173*, 219–237.

[32] M.-R. Li, J. Chen, G.-C. Wang, *J. Phys. Chem. C* **2016**, *120*, 14198–14208.

[33] E. Martono, M.P. Hyman, J.M. Vohs, *Phys. Chem. Chem. Phys.* **2011**, *13*, 9880–9886.

[34] Y.T. Law, W.H. Doh, W. Luo, S. Zafeiratos, *J. Mol. Catal. A* **2014**, *381*, 89–98.

[35] W. Luo, A. Asthagiri, *Catal. Sci. Technol.* **2014**, *4*, 3379–3389.

[36] S.S.-Y. Lin, D.H. Kim, M.H. Engelhard, S.Y. Ha, *J. Catal.* **2010**, *273*, 229–235.

[37] M.P. Hyman, E. Martono, J. Vohs, *J. Phys. Chem. C* **2010**, *114*, 16892–16899.

[38] L. del Río, G. Marbán, *Appl. Catal., B* **2014**, *150–151*, 370–379.

[39] R. Espinal, E. Taboada, E. Molins, R.J. Chimentao, F. Medina, J. Llorca, *Appl. Catal., B* **2012**, *127*, 59–67.

[40] E. Varga, P. Pusztai, L. Óvári, A. Oszkó, A. Erdőhely, C. Papp, H.P. Steinrück, Z. Kónya, J. Kiss, *Phys. Chem. Chem. Phys.* **2015**, *17*, 27154–27166.

[41] L. Qiu, F. Liu, L. Zhao, Y. Ma, J. Yao, *Appl. Surf. Sci.* **2006**, *252*, 4931–4935.

[42] S.M.F. Shahed, T. Hasegawa, Y. Sainoo, Y. Watanabe, N. Isomura, A. Beniya, H. Hirata, T. Komeda, *Surf. Sci.* **2014**, *628*, 30–35.

[43] A.M. da Silva, L.V. Mattos, J.P. de Breejen, J.H. Bitter, K.P. de Jong, F.B. Noronha, *Catal. Today* **2011**, *164*, 234–239.

[44] S.M. de Lima, A.M. da Silva, U.M. Graham, G. Jacobs, B.H. Davis, L.V. Mattos, F.B. Noronha, *J. Catal.* **2009**, *268*, 268–281.

[45] T. Mondal, K.K. Pant, A.K. Dalai, *Int. J. Hydrogen Energy* **2015**, *40*, 2529–2544.

[46] T. Montini, M. Melchionna, M. Monai, P. Fornasiero, *Chem. Rev.* **2016**, *116*, 5987–6041.

[47] S.S.-Y. Lin, D.H. Kim, S.Y. Ha, *Appl. Catal., A* **2009**, *355*, 69–77.

[48] E. Martono, J.M. Vohs, *ACS Catal.* **2011**, *1*, 1414–1420.

[49] W. Xu, Z. Liu, A.C. Johnston-Peck, S.D. Senanayake, G. Zhou, D. Stacchiola, E.A. Stach, J.A. Rodriguez, *ACS Catal.* **2013**, *2*, 975−984.

[50] H. Song, X. Bao, C.M. Hadad, U.S. Ozkan, *Catal Lett.* **2011**, *141*, 43–54.

[51] H. Song, L. Zhang, R.B. Watson, D. Braden, U.S. Ozkan, *Catal. Today* **2007**, *129*, 346–354.

[52] S.S.-Y. Lin, H. Daimon, S.Y. Ha, *Appl. Catal., A* **2009**, *366*, 252–261.

[53] A.M. de Silva, L.O.O. da Costa, K.R. de Souza, L.V. Mattos, F.B. Noronha, *Catal. Commun.* **2010**, *11*, 736–740.

[54] A.M. da Silva, K.R. de Souza, G. Jacobs, U.M. Graham, B.H. Davis, L.V. Mattos, F.B. Noronha, *Appl. Catal. B* **2011**, *102*, 94–109.

[55] S.M. de Lima, I.O. da Cruz, G. Jacobs, B.H. Davis, L.V. Mattos, F.B. Noronha, *J. Catal.* **2008**, *257*, 356–368.

[56] S.M. de Lima, A.M. Silva, I.O. da Cruz, G. Jacobs, B.H. Davis, L.V. Mattos, F.B. Noronha, *Catal. Today* **2008**, *138*, 162–168.

[57] S.M. de Lima, A.M. Silva, U. M. Graham, G. Jacobs, B. H. Davis, L.V. Mattos, F.B. Noronha, *Appl. Catal., A* **2009**, *352*, 95–113.

[58] A. Casanovas, M. Roig, C. de Leitenburg, A. Trovarelli, J. Llorca, *Int. J. Hydrogen Energy* **2010**, *35*, 7690–7698.

[59] K.-S. Kim, H.-R. Seo, S.Y. Lee, J.-G. Ahn, W.Ch. Shin, Y.-K. Lee, *Top Catal.* **2010**, *53*, 615–620.

[60] M. Greluk, M. Rotko, A. Machocki, *Catal. Lett.* **2016**, *146*, 163–173.

[61] A. Machocki, T. Ioannides, E. Papadopoulou, B. Banach, *Fuel Processing Technol.* **2016**, *148*, 341–349.

[62] M. Greluk, G. Słowik, M. Rotko, A. Machocki, *Fuel* **2016**, *183*, 518–530.

[63] E. Varga, K. Baán, G.F. Samu, A. Erdőhelyi, A. Oszkó, Z. Kónya, J. Kiss, 2016 doi:10.1007/s10562-016-1809-3.

[64] J.Y.Z. Chiou, W.-Y. Wang, S.-Y. Yang, C.-L. Lai, H.-H. Huang, C.-B. Wang, *Catal Lett.* **2013**, *143*, 501–507.

[65] J.-W.Snoeck, G.F. Froment, M. Fowles, *Ind. Eng. Chem. Res.* **2002**, *41*, 3548–3556.

[66] A.G. Gayubo, J. Vicente, J. Ereña, C. Montero, M. Olazar, J. Bilbao, *J. Catal. Lett.* **2014**, *144*, 1134–1143.

[67] K. Vasudeva, N. Mitra, P. Umasankar, S.C. Dhingra, *Int. J. Hydrogen Energy* **1996**, *21*, 13–18.

[68] V. Mas, R. Kiproes, N. Amadeo, M. Laborde, *Int. J. Hydrogen Energy* **2006**, *31*, 21–28.

[69] E.Y. García, M. Laborde, *Int. J. Hydrogen Energy* **1991**, *16*, 307–312.

[70] F. Diehl, A.Y. Khodakov, *Oil Gas Sci. Technol.* **2009**, *64*, 11–24.

[71] Y.-J. Wang, H. Dong, G.-M. Lyu, H.-Y. Zhang, J. K., L.-Q. Kang, J.-L.Teng, Li.-D. Sun, R. Si, J. Zhang, Y.-J.Liu, Y.-W. Zhang, Y.-H.Huang, C.-H. Yan, *Nanoscale* **2015**, *7*, 13981–13990.

[72] M.C. Biesinger, B.P. Payne, A.P. Grosvenor, L.W.M. Lau, A.R. Gerson, R.St.C. Smart, *Appl. Surf. Sci.* **2011**, *257*, 2717–2730.

[73] P. Rybak, B. Tomaszewska, A. Machocki, W. Grzegorczyk, A. Denis, *Catal. Today* **2011**, *176*, 14–20.

[74] M. Araque, J.C. Vargas, Y. Zimmermann, A.-C. Roger, *Int. J. Hydrogen Energy* **2011**, *36*, 1491–1502.

[75] G.R. Rao, B.G. Mishra, *Bull. Catal. Soc. India* **2003**, *2*, 122–134.

[76] H. Song, B. Mirkelamoglu, U.S. Ozkan, *Appl. Catal., A* **2010**, *382*, 58–64.

[77] H. Idriss, *Platinum Metals Rev.* **2004**, *48*, 105–115.

[78] X.D. Hou, Y.Z. Wang, Y.X. Zhao, *Catal. Lett.* **2008**, *123*, 321–326.

[79] J. El Fallah, S. Boujana, H. Dexpert, A. Kiennemann, J. Majerus, O. Touret, F. Villain, F. Le Normand, *J. Phys. Chem.* **1994**, *98*, 5522–5533.

[80] M. Romeo, K. Bak, J. El. Fallah, F. Le Normand, L. Hilarie, *Surf. Interface Anal.* **1993**, *20*, 508–512.

[81] E. Paparazzo, G.M. Ingo, J. Electron. *Spectr. Relat. Phenom* **1998**, *87*, 301–304.

[82] E. Paparazzo, G.M. Ingo, N. Zacchetti, *J. Vac. Sci. Techn. A* **1991**, *9*, 1416–1420

[83] E. Paparazzo, *Surf. Sci. Lett.* **1990**, *234*, L253–L258.

[84] L. Óvári, S.K. Calderon, Y. Lykhach, J. Libuda, A. Erdőhelyi, C. Papp, J. Kiss, H.-P. Steinrück, *J. Catal.* **2013**, *307*, 132–139.

[85] J. Rynkowski, J. Farbotko, R. Touroude, L. Hilarie, *Appl. Catal. A* **2000**, *203*, 335–348.

[86] Z. Liu, T. Duchoň, H. Wang, D.C. Grinter, I. Waluyo, J. Zhou, Q. Liu, B. Jeong, E.J. Crumlin, V. Matolín, D.J. Stacchiola, J.A. Rodriguez, S.D. Senanayake Phys. Chem. Chem. Phys. **2016**, *18*, 16621–16628

[87] M. Konsolakis, M. Sgourakis, S.A.C. Carabineiro, *Appl. Surf. Sci.* **2015**, *341*, 45–54.

[88] A. Pfau, K.D. Schierbaum, *Surf. Sci.* **1994**, *321*, 71–80.

[89] D.R. Mullins, M.D. Robbins, J. Zhou, *Surf. Sci.* **2006**, *600*, 1547–1558.

[90] F. Larachi, J. Pierre, A. Adnot, A. Bernis, *Appl. Surf. Sci.* **2002**, *195*, 236–250.

[91] D. Cappus, C. Xu, D. Ehrlich, B. Dillmann, C.A. Ventnce Jr., K. Al Shamery, H. Kuhlenbeck, H.-J. Freund, *Chem. Phys.* **1993**, *177*, 533–546.

[92] D.A. Creaser, P.G. Harrison, *Catal. Lett.* **1994**, *23*, 13–24.

[93] B.E. Koel, G. Praline, H.-I. Lee, J.M. White, *J. Electron. Spectrosc. Relat. Phenom.* **1980**, *21*, 31–46.

[94] M. Sun, L. Wang, B. Feng, Z. Zhang, G. Lu, Y. Guo, *Catal. Today* **2011**, *175*, 100–105.

[95] J.L. Ayastuy, A. Gurbani, M.P. González-Marcos, M.A. Gutiérrez-Ortiz, *Int. J. Hydrogen Energy* **2012**, *37*, 1993–2006.

[96] T.L. Westover, A.D. Franklin, B.A. Cola, T.S. Fisher, R.G. Reifenberger, *J. Vac. Sci. Techn., A* **2010**, *28*, 423–434.

[97] Z. Hou, O. Yokota, T. Tanaka, T. Yashima, *Catal. Lett.* **2003**, *87*, 37–42.

[98] A.V. Shchukarev, D.V. Korolkov, *CEJC* **2004**, *2*, 347–362.

[99] J. Iranmahboob, D.O. Hill, H. Toghian, *Appl. Surf. Sci.* **2001**, *185*, 72–78.

[100] B. Lamontagne, F. Semond, D. Roy, *J. Electron. Spectrosc. Relat. Phenom.* **1995**, *73*, 81–88.

[101] G. Pirug, O. Müller, H. P. Bonzel, *Surf. Sci.* **1993**, *73*, 145–154.

[102] M. Carlsson, *Johnson Matthey Technol. Rev.* **2015**, *59*, 313–318.

[103] H.P. Bonzel, H.J. Krebs, *Surf. Sci.* **1981**, *109*, L527–L531.

[104] H.P. Bonzel, G. Broden, H.J. Krebs, *Appl. Surf. Sci.* **1983**, *16*, 373–394.

[105] G. Maniak, P. Stelmachowski, A. Kotarba, Z. Sojka, V. Rico-Pérez, A. Bueno-López, *Appl. Catal., B* **2013**, *136–137*, 302–307.

[106] L. del Río, G. Marbán, *Appl. Catal., B* **2012**, *126*, 39–46.

[107] S. Davidson, J. Sun, Y. Wang, *Top Catal.* **2013**, *56*, 1651–1659.

[108] D. Teschner, A. Wootsch, O. Pozdnyakova, J. H. Sauer, A. Knop-Gericke, R. Schlögl, *React. Kinet. Catal. Lett.* **2006**, *87*, 235–247.

[109] L. Xu, Y. Ma, Y. Zhang, B. Chen, Z. Wu, J. Jiang, W. Huang, *J. Phys. Chem. C* **2010**, *114*, 17023–17029.

[110] T.-L. Chen, D.R. Mullins, *J. Phys. Chem. C* **2011**, *115*, 3385–3392.

[111] E. de Smit, F.M.F. de Groot, R. Blume, M. Hävecker, A. Knop-Gericke, B.M. Weckhuysen, *Phys. Chem. Chem. Phys.* **2010**, *12*, 667–680.

[112] N. Hou, Y. Zhang, M. Meng, *J. Phys. Chem. C* **2013**, *117*, 4089−4097.

[113] Y. Zhang, M. Meng, F. Dai, T. Ding, R. You, *J. Phys. Chem. C* **2013**, *117*, 23691−23700.

[114] W. Wang, Y.Q. Wang, *Int. J. Energy Res.* **2008**, *32*, 1432–1443.

[115] X.-D. Zhou, W. Huebner, *Appl. Phys. Lett.* **2001**, *79*, 3512–3514.

[116] X. Wan, D. Goberman, L.L. Shaw, G. Yi, G.-M. Chow, *Appl. Phys. Lett.* **2010**, *96*, 123108.

[117] A.L.M. da Silva, J.P. den Breejen, L.V. Mattos, J.H. Bitter, K.P. de Jong, F.B. Noronha, *J. Catal.* **2014**, *318*, 67–74.

[118] S. Helveg, J. Sehested, J.R. Rostrup-Nielsen, *Catal. Today* **2011**, *178*, 42–46.

[119] L.V. Mattos, G. Jacobs, B.H. Davis, F.B. Noronha, *Chem. Rev.* **2012**, *112*, 4094–4123.

[120] G. Słowik, A.Gawryszuk-Rżysko, M. Greluk, A. Machocki, Catal Lett. **2016**, 146, 2173–2184.

10.1002/cctc.201601343


WILEY-VCH

## Entry for the Table of Contents

Layout 1:

# FULL PAPER



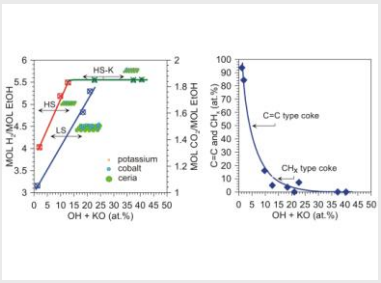


*Sylwia Turczyniak, Magdalena Greluk, Grzegorz Słowik, Wojciech Gac, Spyridon Zafeiratos, and Andrzej Machocki*

***1 – 21***

**The surface state and the catalytic performance of $Co/CeO_2$ catalysts in the steam reforming of ethanol**